RICE UNIVERSITY

A Time-of-Flight Spectrometer for Fast Neutron Physics

by

Richard Keyes

A THESIS SUBMITTED
IN PARTIAL FULFILLMENT OF THE
REQUIREMENTS FOR THE DEGREE OF

MASTER OF ARTS

Thesis Director's Signature:

G C Phillips

Houston, Texas

June, 1965

ABSTRACT

A time-of-flight spectrometer is described that was developed to further the study of the interactions of fast neutrons with nuclei at the Bonner Nuclear Laboratory of the Rice University. A transistorized time-to-pulse height converter utillizing avalanche-mode threshold discrimination and pulse shaping circuits is described. The results of resolution and linearity tests obtained with Na^{22} and Co^{60} γ - sources are shown. Data from neutron-proton scattering experiments are presented to indicate the efficiency of the time-of-flight system.

Richard Keyes

TABLE OF CONTENTS

I. INTRODUCTION

It is not possible to accelerate or deflect neutrons, and consequently neutron beams must be generated from nuclear reactions. Likewise, neutrons do not cause ionizations and their presence must be detected by the result of nuclear reactions which produce detectable effects. As a result, the process of neutron detection involves several stages in which the efficiency and characteristics of each reaction must be known to make accurate energy and cross-section measurements.

The neutron does have a long effective range due to its lack of ionizing properties, and it is feasible to measure its energy over a given path length by the measurement of the time required to travel the path. The path may be in air at normal atmospheric pressure with a small cross-section for scattering along the path and consequent loss of energy or change of direction. It is apparent that the time-of-flight method for energy determination is independent of the reaction used to detect the presence of the neutron as long as sufficient results of the reaction are noticed to mark the event in time. Therefore, especially in the measurement of the energy of fast neutrons within the energy range of 0.5 to 10 MeV, the time-of-flight neutron spectrometer has become the most generally useful instrument for energy definition. The detectable effect of the reaction producing the neutrons may be used to mark the start of the time interval and a reaction from a neutron scatterer at the end of the path may be detected as the stop signal to terminate the time interval.

A 1 MeV neutron has a velocity of 1.4 centimeters per nanosecond, and in order to measure energies of fast neutrons to an accuracy of a few percent with path lengths of a few meters, the time variations of the detectable signal from the neutron reaction must be of the order of a nanosecond or less. Recoil protons from elastically scattered neutrons irradiating an organic scintillator coupled to a fast photomultiplier tube provides a means of marking the event of a neutron interaction at the end of the path with a time varation of one or two nanoseconds. The initial time may be determined to similar precision by either signals from a pulsed beam causing the initial reaction or the detection of an associated particle or gamma ray.

While energy determinations within a few percent can be made by the time-of-flight technique without detailed consideration of the neutron reaction, except for a knowledge of the energy of the recoil particle and perhaps its spacial distribution, the determination of neutron cross-sections does require a knowledge of the properties of the neutron reaction causing the timing event signals. The overall performance of the time-of-flight system for determining neutron cross-sections can be expressed in a measurement of the efficiency of the system. If the system could record every neutron event that occurs within its path geometry, its efficiency would be 100%. However, there is a definite probability that neutron events will not be recorded mainly due to the indeterminate amount of energy deposited in the recoil scintillator which causes pulse heights below the threshold of the system and the probability that a neutron will pass through the scintillator without scattering from a proton. Therefore it is apparent that the efficiency will at least be a function of the incident neutron energy, the threshold levels of the timing event inputs of the system, and the size of the scintillator. The efficiency of the time-of-flight system described has been measured by scattering neutrons by protons and comparing the experimental yields with the known cross-section for neutron-proton scattering over an energy range of 0.5 to 4 MeV.

II. APPARATUS

Time-To-Pulse Height Converter

It is possible to measure the time between two events by charging a capacitor with a constant current initiated by the first or start event and removed by the second or stop event. The voltage across the capacitor is proportional to the amount of charge accumulated during the time interval between events. This method of current integration is necessary when the time between the events is too short to allow direct counting of timing pulses between events. When the time between events is in order of a few nanoseconds, it is presently not feasible to turn an oscillator on and off by the events and count the number of periods with a resolution of the order of a tenth of a nanosecond because of the lack of practical UHF digital techniques and components. However, with presently available conponents, it is possible to attain a repeatability and resolution of a few tenths of a nanosecond by generating a voltage proportional to the time interval. Once the voltage has been stored on a capacitor, it is then possible to hold it for a time sufficiently long to allow presently available instrumentation to convert the voltage level to a digital representation for spectrum analysis.

However, uncertainities in determining the time at which an event occurs normally limits the resolution that can be attained regardless of the method used for time measurement. Time variations caused by variations of amplitude and a finite risetime of the pulse defining a physical event are difficult to reduce to less than a nanosecond. Typically for fast neutron detection, plastic scintillators offer the best characteristics of available particle detectors and when coupled to a fast photomultiplier tube produce a pulse output with a rise time approaching two nanoseconds, a fall time approaching ten nanoseconds, and a half-width duration of about two nanoseconds. However, since it is the recoil proton of variable energy that produces the scintillation, the pulse defining the elastically scattered neutron event will be of varying amplitude and this effect will produce time uncertainities of a few nanoseconds with a threshold circuit triggering along the leading edge of the pulse.

Several methods have been used to correct for the time shift associated with pulse amplitude variations[1) 2)]. A popular scheme[3)] utillized with slower rise time pulses is the single or double differentiation of the input pulse to define the event time at the apparent centroid of the pulse if it is symmetrical. This tends to reduce time shifts in determining physical events by an order of magnitude; however, it is difficult to apply the technique to a two nanosecond pulse requiring differentiation that produces a one nanosecond pulse that is linear over more than a decade of amplitude range without excessive attenuation. Any nonlinearity in the pulse shaping will produce a corresponding shift in the apparent centroid. As better components and techniques become available, the method of differentiating the input pulse before determining the threshold should be capable of time shifts less than a few tenths of a nanosecond with a two nanosecond pulse. To accomplish this order of differentiation, the input circuitry must have a frequency response approaching two gigacycles. While wave guide apparatus is normally employed in this range, coaxial techniques are still feasible, but excessive losses in passive linear elements become difficult to overcome. Even so, pulse differentiation would tend to eliminate the time shift rather than try to compensate for it as the other methods that have been suggested.

Since single or double differentiation of the nanosecond pulses will probably become feasible with further development, the present time-to-pulse height converter employs only one technique[4)] from the various suggested methods to attempt to reduce time shifts with leading edge threshold detection. Two pulse threshold descriminators are connected to the same input pulse line with one threshold level set down in the photomultiplier noise region and the other threshold level set just above the noise region. The signal from the lower threshold is delayed by at least the rise time of the input pulse and then placed in coincidence with the signal from the upper threshold before initiating the time signal. This method has the advantage of triggering with the lowest possible signal while defining a leading edge time that is not subject to the major time shift that occurs when the pulse amplitude approaches the threshold level. This time shift around threshold is very much greater than the rise time of the input pulse and is apparently caused by the tendency of the threshold circuit to integrate a low level pulse over its time duration up to a sufficient level to trigger the discriminator. For the pulse shapes obtained from the plastic scintillators, the time duration is at least six nanoseconds. The use of two threshold circuits reduces the time shift to slightly less than two nanoseconds. With two sets of threshold systems required to define a start event and a stop event, in the worst case the time shift is doubled. Even so, the resulting time spread determined by experiment with the threshold system indicated an experimental resolution of less than two nanoseconds with a Co^{60}-γ source and less than four nanoseconds with elastically scattered neutrons as measured by the half-width of the peaks in the time-of-flight spectrum.

The threshold coincidence signals from both the start event input and the stop event input each trigger a pulse shaper to generate a pulse a few hundred nanoseconds long. Both the start event pulse shaper and the stop event pulse shaper generate identical pulses. The outputs of the two pulses shapers are placed in coincidence to provide a pulse-width proportional to the overlap time of the shaper outputs. It is this pulse that determines the integration time of the charging capacitor to accomplish the time-to-pulse height conversion. Since the overlap pulse is symmetrical with regard to exchange of start and stop events, it is necessary to prevent the occurrence of a stop threshold coincidence signal unless a start threshold coincidence signal has occurred. This is accomplished by placing a third condition on the stop threshold coincidence circuit. The output of the start event pulse shaper is returned to the stop threshold coincidence circuit to prevent the stop event pulse shaper from triggering at any time except during the period that a start event pulse has been generated from the shaper. This allows a stop event signal to be registered only within a few hundred nanoseconds after the start event. A pulse amplifier is used after the integrating capacitor to buffer the resulting pulse of varying amplitude proportional to overlap time and provide a sufficiently low driving point impedance for a 50 ohm coaxial cable. A pulse shaping filter is also included to provide a pulse to the spectrum analysers of approximately 0.5 microseconds rise time and 5 microseconds fall time.

Threshold Discrimination

To provide a pulse of uniform amplitude and time duration from an input pulse of varying amplitude and time duration defining the occurrence of an event, a single transistor operating in an avalanche-mode breakdown condition[5)] has been used as a pulse threshold discriminator in the time-to-pulse height converter designed at Rice University. The main advantage of the avalanche-mode threshold circuit over a tunnel diode threshold circuit over a tunnel diode threshold circuit is a higher input impedance and a higher degree of isolation between input and output. The stable sensitivity of the avalanche circuit however is slightly less than reported for tunnel diode circuits, and a noticeable feedback signal will occur on the input line when the circuit triggers if the source impedance is not zero. The stable input sensitivity of the avalanche-mode threshold circuit can be adjusted from less than 50 millivolts to a few volts which is adequate to cover the range of output pulses from the anode circuit of photomultiplier tubes used in scintillation counters in fast neutron physics. An emitter-follower circuit with an RC filter is placed in the input line to reduce the feedback signal on the input so that more than one threshold circuit may be connected to a photomultiplier tube.

The basic scheme for the discriminator is shown in Figure 1. The supply voltage and resistors R_1 and R_2 determine the breakdown current through the base and collector of Q_1 assuming the collector load is small. The delay line in the emitter is charged through resistors R_1, R_2, and R_3 to approximately BV_{CBO}, however the base voltage is held equal to or more positive than the emitter voltage and in the steady state, Q_1 is non-conducting and operating in the avalanche region of its characteristic curves. If a negative pulse greater than the base-to-emitter

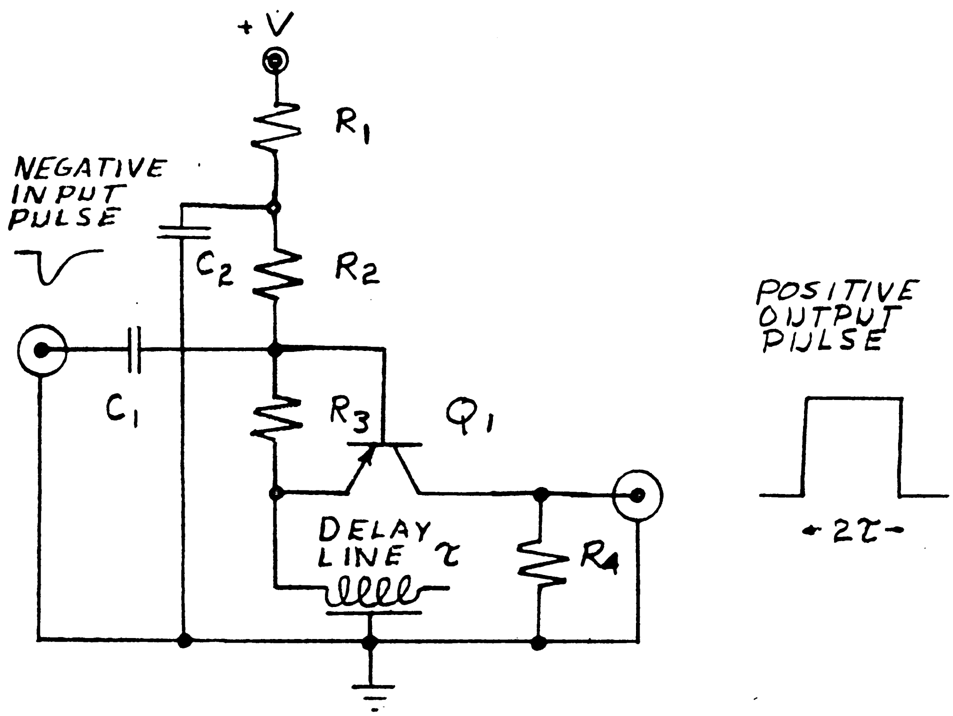

FIGURE 1

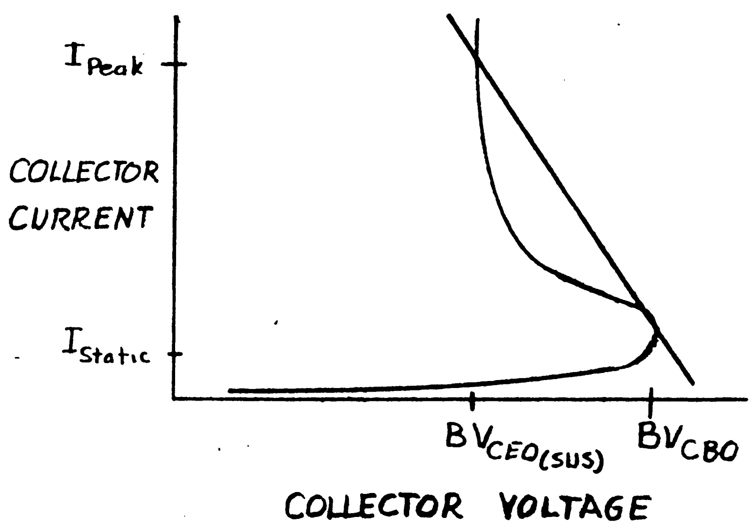

FIGURE 2

junction voltage is applied through capacitor C_1 to the base of Q_1, the transistor will begin to conduct current from the stored charge on the delay line through the emitter-to-collector junction. Once the transistor begins to conduct it will breakdown by alpha multiplication[5] avalanche until $BV_{CEO(SUS)}$ is reached and a constant current will be supplied to the load R_4 by the delay line proportional to the difference between BV_{cbo} and $VB_{CEO(SUS)}$. For the circuit to function, the transistor Q_1 must exhibit a second breakdown condition as shown in Figure 2. The most common type of transistor exhibiting good avalanche breakdown characteristics is the germanium mesa transistors. Some epitaxial planar transistors provide fast avalanche switching as demonstrated by such types similar to the 2N709 and the 2N3035. The germanium mesa type 2N955A was found to exhibit a stable operation at a sensitivity of 50 millivolts with a very sharp rise and fall time less than 0.5 nanoseconds without requiring a high supply voltage since its BV_{CBO} is around 20 volts. However, it is an NPN type transistor and in the application considered it was necessary to accept a negative input pulse without adding a stage of inversion. The PNP germanium mesa type 2N705 was finally used in the prototype with very little loss of apparent rise and fall time. Also it was found that the delay line should have a value of a few hundred ohms to best match a 50 ohm load with the value of saturation resistance of the 2N705 which is in series with the load. Since R_1 is a large resistance to limit the breakdown current, the repetition rate is limited by the ability of the circuit to recharge the delay line between input pulses. Since in nuclear physics applications, the time between events may be less than the average repetition rate, capacitor C_2 was added to provide some recharging current through R_2 and R_3 to the delay line. The load on the input however is determined by R_2 and R_3 in parallel, placing a lower limit on the value of resistances used and consequently on the time interval between pulses. For the values decided upon for the prototype, a maximum continuous rate greater than 100 KC was possible with a 5 nanosecond output pulse and 1 K input impedance with about 100 nanoseconds required to charge the delay line from C_2.

The complete threshold discriminator circuit is shown in Figure 3. Potentiometer R_5 offers an adjustment of the input sensitivity from less than 50 millivolts to a few volts. As the voltage is increased on the slider arm of the potentiometer, the voltage drop across R_3 is decreased to zero with the emitter-to-collector leakage being supplied through R_5 and the base-to-collector leakage through R_2 in the steady state condition. As the potentiometer is further increased, the voltage on the emitter will become sufficiently more positive than the base to cause the transistor to avalanche and discharge the delay line into the load. The circuit will then be unstable and oscillate with a repetition rate proportional to the recharging time constant of the circuit. As the potentiometer is backed down, the oscillation will cease and a stable triggering point of 40 to 50 millivolts will be reached. If the input pulse is longer than a few nanoseconds, an increased sensitivity will be noticed due to the tendency of the threshold circuit to apparently integrate the input signal up to a sufficient value to trigger the circuit as a considerable delay in the output pulse is noticed for input pulse levels less than 40 millivolts with greater than ten nanoseconds duration. This variable delay band is less than about 10 millivolts and above 50 millivolts, the delay is fixed at around a nanosecond with the circuit triggering along the rise time of the pulse if it is greater than a nanosecond.

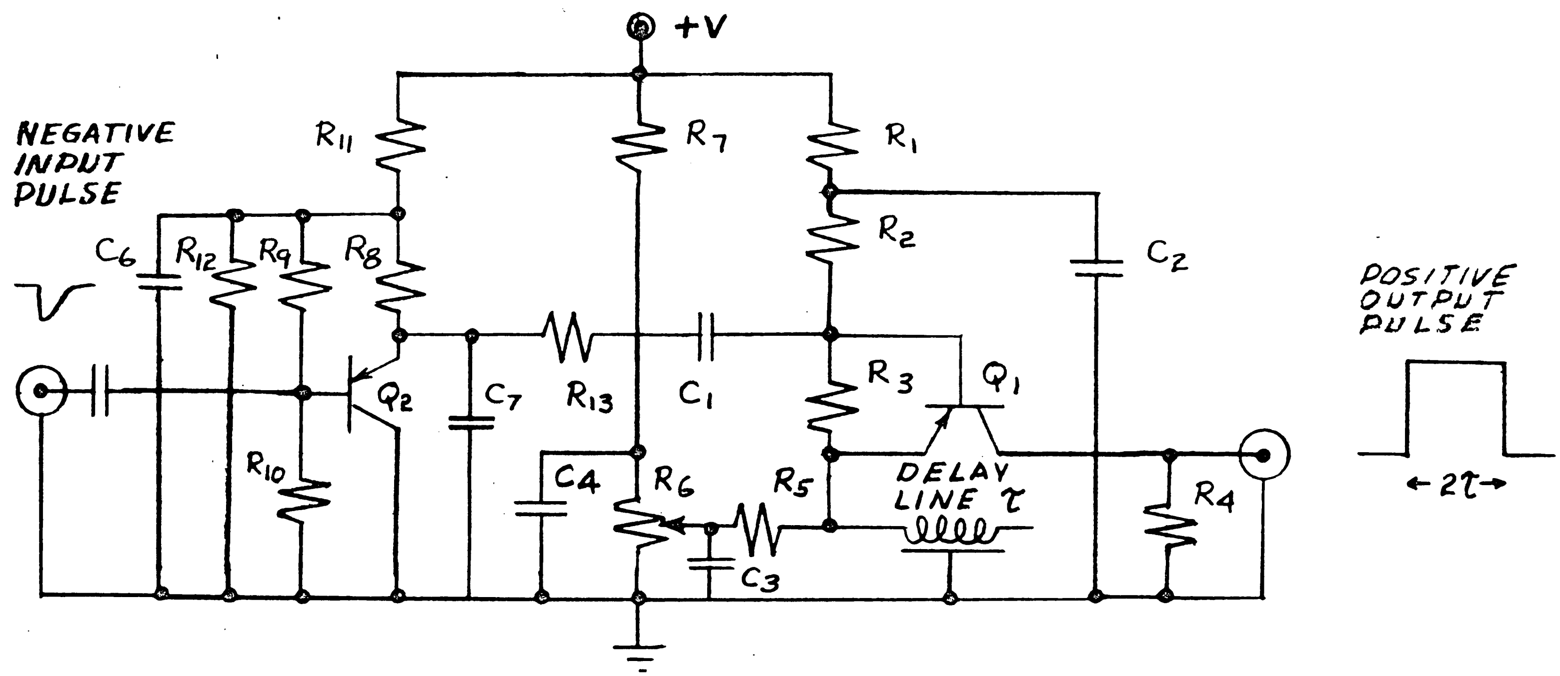
+V
NEGATIVE
INPUT
PULSE
R11
R7
R1
R2
C6
R12
R9
R8
C2
POSITIVE
OUTPUT
PULSE
Q2
C7
R13
C1
R3
Q1
R10
C4
R6
R5
DELAY
LINE τ
R4
C3
2τ

FIGURE 3

The input sensitivity will decrease if the rise time of the input pulse is slow enough to allow the delay line to discharge through R_3 to prevent the base from becoming negative with respect to the emitter. Therefore the sensitivity, repetition rate, and duration of output pulse are all interrelated. The 50 millivolt sensitivity and 100 KC repetition rate were attained with an input pulse of a few nanoseconds rise time and an output pulse of 5 nanoseconds. If the length of the delay line were increased, the same sensitivity could be obtained with an input pulse of longer rise time with a corresponding reduction of the maximum possible continuous repetition rate. The rise and fall time are not dependent on the length of the delay line but only on its response characteristics and the impedances of the circuit. The rise and fall times obtainable from avalanche-mode circuits is generally not very dependent on transistor frequency response characteristics except as they relate to circuit impedances around them. A transistor with ten times poorer frequency response was found to still provide output pulses of 100 nanoseconds duration with a nanosecond rise time.

The emitter follower Q_2 is placed in the input line to prevent the feedback to the input of a pulse that occurs when the discriminator triggers and the base voltage of Q_1 changes from BV_{CBO} to $BV_{CES(SUS)}$ in less than a nanosecond. An RC filter is also placed in the circuit to further reduce feedback current. The emitter follower is capable of driving the capacitor C_7, and the series resistor R_{13} causes only a small attenuation with the high input impedance of the discriminator. However, in the reverse direction, the feedback signal is greatly attenuated by the RC filter. With the circuit as shown, a spike of less than 20 millivolts appears on a 50 ohm input line when the circuit triggers. The filter of R_5 and C_3 is necessary to decouple the potentiometer from the sharp voltage changes that occurs on the emitter of Q_1 to prevent radiation or pickup in the wirewound, 10 turn potentiometer that was used to set the threshold level. R_5 not only decouples the delay circuit but also places a lower and upper limit to the amount of current that can be supplied to the emitter circuit when varying the threshold levels to prevent accidental damage to the transistor by shorting the emitter to the supply voltage.

Coincidence And Pulse Shaping Circuits

The coincidence section receives the output signals from the lower and upper threshold discriminators connected to one of the timing event inputs and provides a signal output only if the two discriminator signals are simultaneously present. The upper threshold signal is 10 nanoseconds wide and occurs if the timing event signal is greater than a preset level above the input noise. The lower threshold is delayed by 10 nanoseconds and is adjusted to trigger on noise as well as a timing event signal. The lower threshold signal must be delayed by at least the rise time of the timing event pulse as it triggers on the leading edge of the timing pulse at a time earlier than the upper threshold signal. With the lower threshold signal delayed, the output of the coincidence circuit always initiates at the lowest possible level of the timing input signal and reduces a major portion of the walk in the leading edge discriminator because of the separation in triggering levels of the upper and lower discriminators. There is no output from the coincidence circuit unless the timing signal is above the noise. However, if it is above the noise, the coincidence output will coincide with the delayed lower level threshold signal which is firmly triggered at a level in the noise and the tendency to walk about the trigger point is overcome. The best choice of the ratio between the upper and lower threshold for good sensitivity and minimum walk was four to one. For a 56AVP photomultiplier tube operating with about 2200 volts, the upper threshold could be set around 200 millivolts without triggering on tube noise. The lower threshold was set to around 50 millivolts (in the noise).

The circuit configuration of the typical coincidence and pulse shaping circuit used in the time-to-pulse height converter is shown in Figure 4. Q_1 and Q_2 of the coincidence circuit are normally held in a conducting state by base current flowing through resistors R_4 and R_5 respectively from the regulated voltage source of the Zener diode CR_1. The output of the coincidence circuit is the common collectors of the two transistors and is normally held at ground by either transistor in the conducting state. When a signal from one of the threshold discriminators is present, it will drain the current that was flowing into the transistor base and cause the transistor to become non-conducting. The discriminator output signals are always positive and greater than about one volt which is enough to remove the base current from Q_1 or Q_2 through R_1 or R_2. However, the output of the coincidence circuit will not change if only one transistor is made non-conducting as the other transistor will hold the output at ground. If both transistors become non-conducting simultaneously, current will cease to flow in L_1 and a voltage across the inductor will be rapidly generated on the coincidence output across L_1 since C_1 holds the other side of L_1 at essentially ac ground. R_8 is included to limit the dc current flowing through the normally conducting transistors. R_7

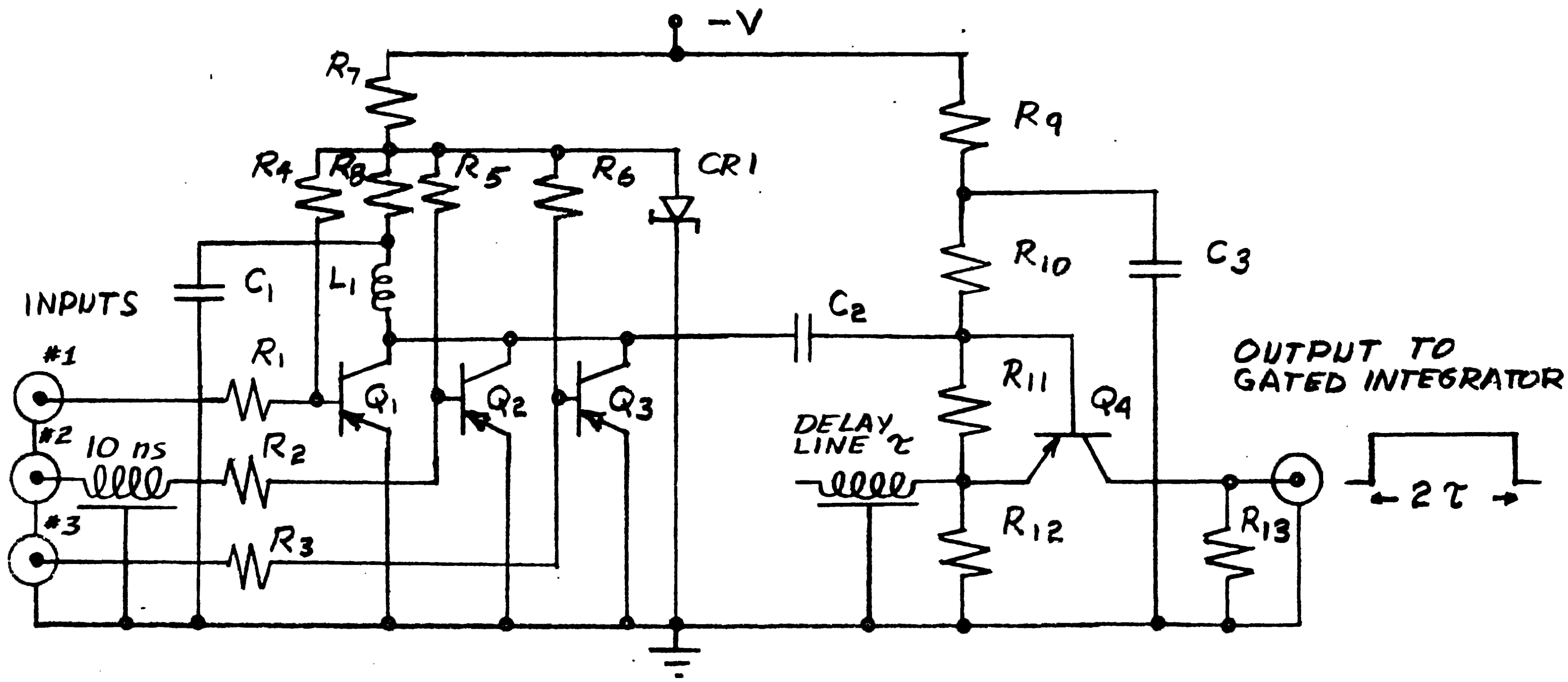

INPUTS: #1 FROM UPPER THRESHOLD

#2 FROM LOWER THRESHOLD

#3 START FEEDBACK PULSE (STOP INPUT SIDE ONLY)

- R_6, R_3, + Q_3 NOT USED ON START SIDE -

FIGURE 4

supplies the required current to the Zener diode to provide a stable and isolated power source for the circuit. On the stop event side of the time-to-pulse height converter, a third coincidence circuit is added to prevent an output from the stop threshold signals unless a start event signal has occurred. This addition consists of R_3, R_6, and Q_3 operating exactly the same as the other two transistor circuits around Q_1 and Q_2. The input to this additional circuit is however a few hundred nanoseconds duration and comes from the output of the start event pulse shaping circuit.

The pulse shaping circuit on both the start and stop event sides of the time-to-pulse height converter are identical and very similar to the input threshold discriminators. The triggering level of the shaping circuit is set to around one volt to prevent an output signal unless a true coincidence occurs. The output line of the coincidence section has noise signals in the order of one-half volt under various conditions of non-coincidence signals appearing from the input discriminators. The delay line of the avalanche-mode triggering circuit used as the pulse shaping circuit is adjusted to a few hundred nanoseconds which determines the time range of the converter. Since the integrator section charges a condenser proportional to the time overlap of the output signals of the start and stop event pulse shaping circuits, the maximum time which the condenser is allowed to charge is just the length of the delay line in each pulse shaping circuit providing that both start and stop event signals occur simultaneously. The condenser will not charge at all if the time delay of the stop event signal is greater than the signal out of the start event pulse shaping circuit. The output signals from both the pulse shaping circuits are adjusted to the same duration by cutting identical delay lines. For durations of a few hundred nanoseconds, the output of the shaping circuits is about one volt positive with a flat top and a rise time of about a nanosecond and a fall time of about two nanoseconds. For the initial experiments, a time duration of 100 nanoseconds was used.

Integrator

To convert the time between the event signals into a proportional pulse height, a gated integrator is used as shown in Figure 5. The gates on the integrator are connected to the outputs of the pulse shaping circuits and open for a period of a few hundred nanoseconds when an event signal triggers its respective pulse shaping circuit. When both gates on the integrator are opened, the integrating capacitor is charged with a constant current, and the resulting voltage across the capacitor is proportional to the overlap time of the outputs of the start and stop event pulse shaper circuits. The maximum voltage to which the capacitor can charge depends on the time duration of the pulse generated in the pulse shaping circuits and occurs when both the start and stop timing event signals are simultaneously received at the inputs of the converter.

The gating section of the integrator is identical to the coincidence circuit described previously. However, instead of an inductor in the collector circuit, only a resistor is used between the Zener diode regulator and the common collectors of the gate. Both transistors in the gating circuit are normally conducting. When the outputs of the pulse shaping circuits overlap, both transistors in the gating circuit become non-conducting, and the current normally flowing through them is diverted to the integrating circuit. The collector circuit of the integrating transistor is a constant current supply for the integrating capacitor which is charged with the current normally diverted to ground through the

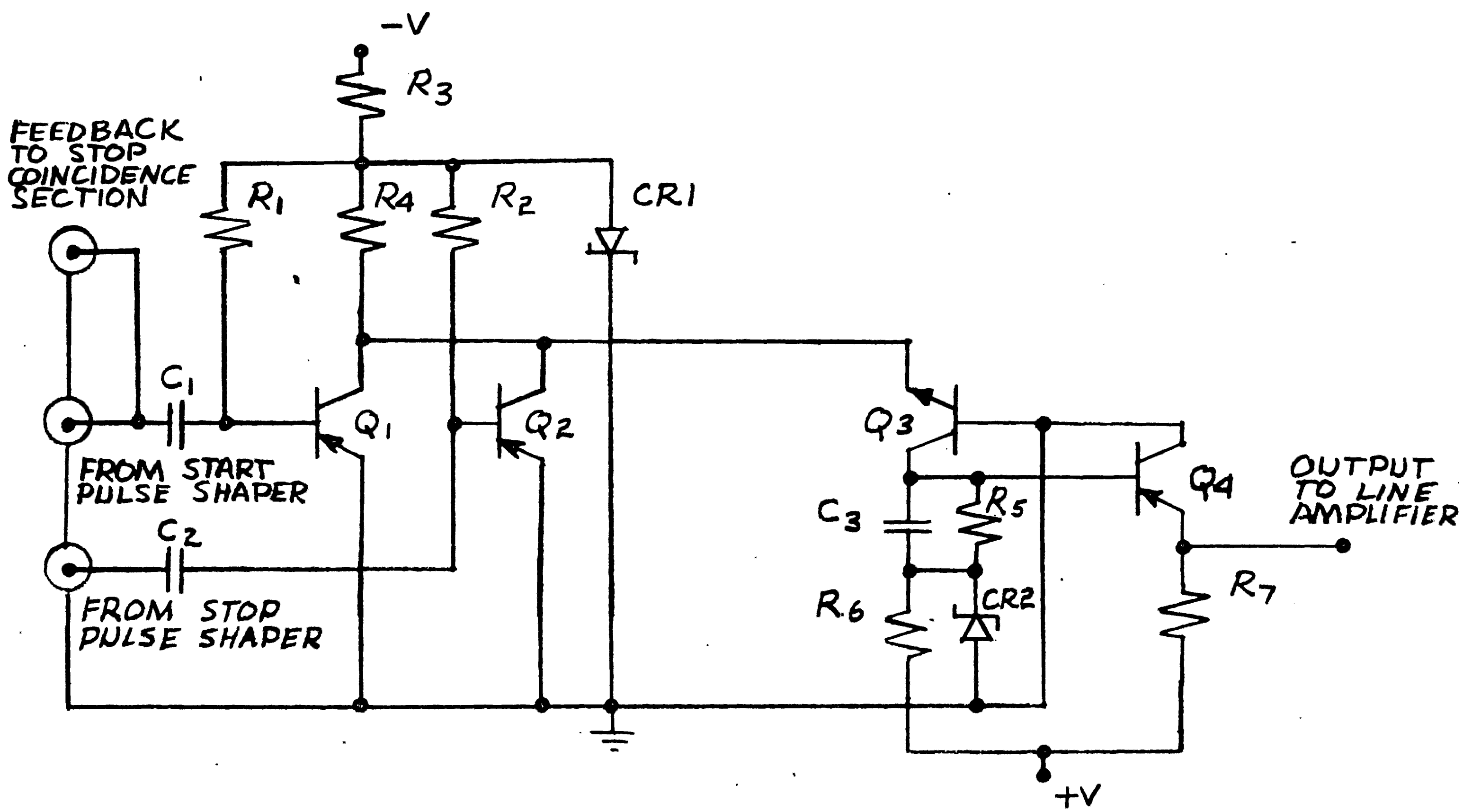

INTEGRATOR

FIGURE 5

gates since the collector-to-emitter voltage drop of the conducting transistors in the gates is less than the emitter-to-base voltage drop of the integrating transistor. The integrating condenser of 1000 picofarads is charged to about one volt in a hundred nanoseconds from the approximately ten milliamperes in the emitter circuit of the transistor. The resistor across the integrating capacitor discharges the capacitor in about ten microseconds but effects the linearity less than one percent. Good linearity is acheived in the integrator even over a one volt output range as the collector current of the transistor is relatively independent of the collector voltage and a constant current flows through the transistor which achieves a constant gain characteristic. The emitter follower decouples the capacitive effects of the filter inserted before the line amplifier to increase the rise time of the integrated signal.

The repetition rate of the time of flight system is limited by the discharge of the integrating capacitor to about 30,000 start pulses per second. When this rate is exceeded, the output pulses from the integrator begin to pile up on each other. The stop side of the converter will stand a repetition rate of about 2 megacycles per second with its limitation due to the recovery time of the threshold discriminator with the ten nanosecond delay line.

Line Amplifier

An isolating amplifier is necessary following the integrator to decouple the integrator from the output circuit and provide a low impedance output to drive a 93 ohm cable between the converter and a pulse height analyzer. Also, the fast rise time of the integrator output signal must be reduced and the signal shaped into a pulse that will be accepted by the analyzer but still remain proportional to the peak height of the integrator signal. The pulse shaping is accomplished in a low pass, RC filter reducing the rise time of the signal to approximately 0.3 microseconds which is constant regardless of the charging time of the integrator as long as it is less than 300 nanoseconds. The low frequency response of the pulse is determined by the coupling capacitor before the filter and the resistor in the emitter of the emitter follower between the integrator and the filter. The fall time of the signal from the filter was adjusted to approximately 5 microseconds.

The circuit of the line amplifier utillizes five transistors in a configuration similar to a quasi-complementary-symmetry amplifier[5)]. The configuration allows a substantial amount of feedback to be placed around the entire amplifier for maximum linearity and stability. The amplifier is dc coupled within the feedback loop for maximum stability of the high current output stages. The two voltage amplifiers have a combined gain in excess of one hundred at a frequency of one megacycle; however, with feedback the amplifier gain is normally reduced to one to provide a maximum signal of one volt to the analyzer. However, if desired, the feedback resistor may be increased to raise the gain to five to provide a maximum output signal of five volts into 93 ohms.

The line amplifier circuit is shown in Figure 6 and the block diagram of the entire converter is shown in Figure 7. The only important construction detail to be mentioned is the careful decoupling of the power supply from the discriminator and coincidence circuits along with careful routing of the ground busses. To minimize inductive pickup and ground noise, all the threshold discriminators and coincidence circuits were

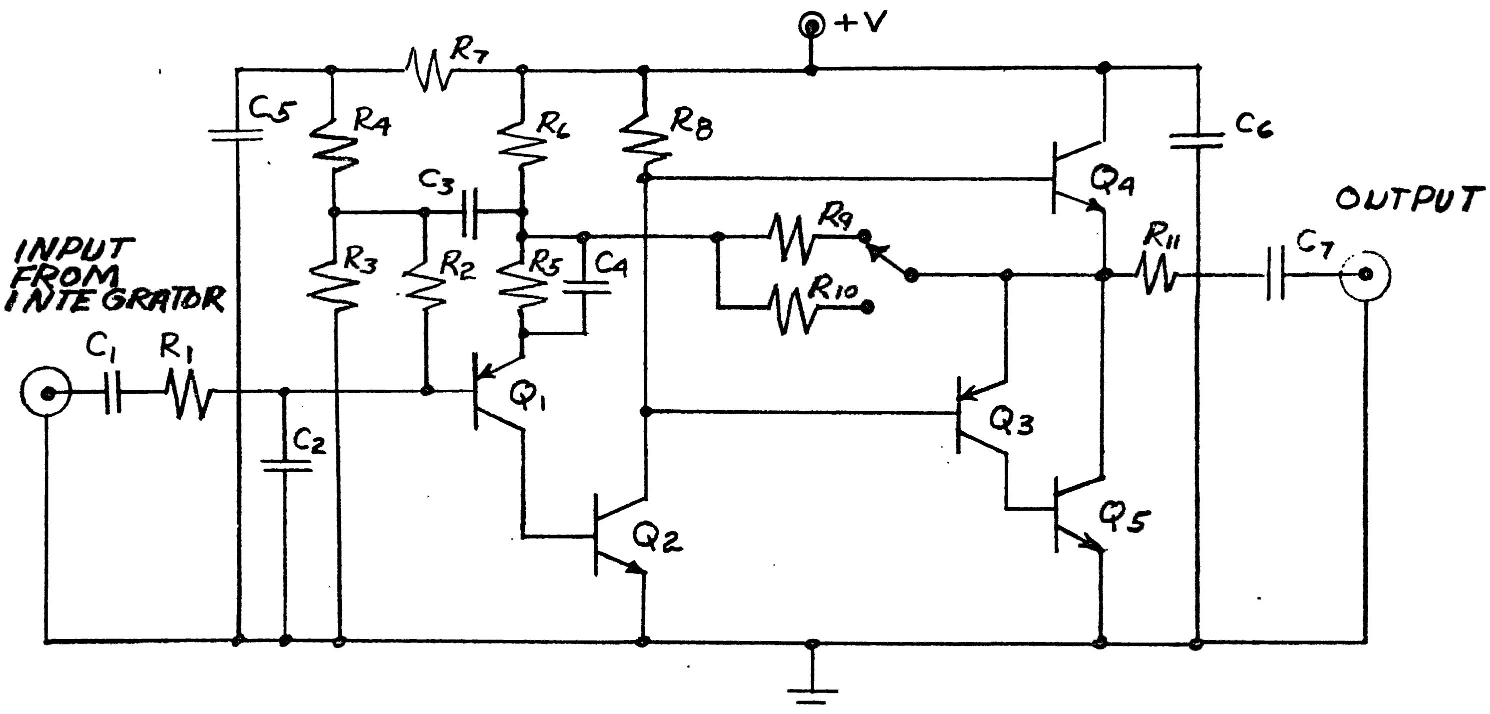

LINE AMPLIFIER

FIGURE 6

TIME - TO - PULSE-HEIGHT CONVERTER

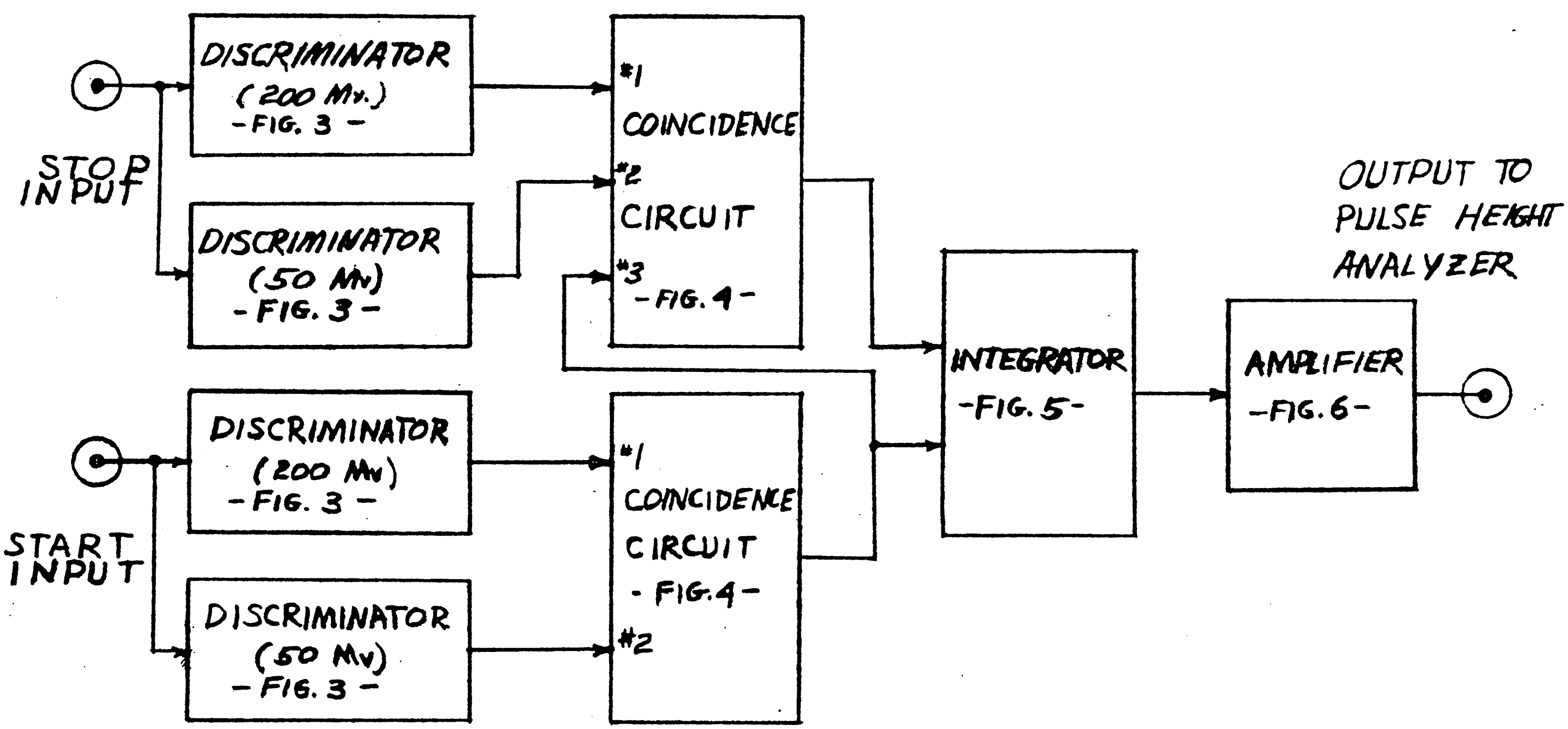

BLOCK DIAGRAM

FIGURE 7

constructed on copper circuit boards with all ground returns soldered directly to the copper. Only after careful decoupling and grounding was it possible to operate the discriminators at a triggering level of fifty millivolts.

Resolution And Linearity Tests

The electronic time resolution of the time of flight system was measured by connecting a fast pulse generator to the start input and then to the stop input through a delay line of adjustable length up to a few hundred nanoseconds. The time event was thus simulated using the one generator with a fixed output level to measure the inherent time stability and noise of the time-to-pulse-height converter. The resulting resolution of 0.56 nanosecond is indicated in Figure 8. This measure of resolution also includes the channel resolution of the computer analyzer system which is between two to three channels wide out of one thousand channels full scale. The time delays of ten nanoseconds were fixed by adding lengths of RG 58/U coaxial cable cut to ten nanosecond delay time between the start and stop inputs. The time linearity measured by this method resulted in an integral linearity within a few percent of the full scale time period.

The variation of time with different amplitude of input signals was measured to be 4 nanoseconds over a 30 to 1 range of input levels and caused the poorer resolution that is found in experiment when the timing signals are derived from scintillation counters. The spread of the time resolution of the time-to-pulse-height converter when connected to two photomultiplier tubes with plastic scintillators and a Na^{22} source placed between the scintillators is found to be 2.5 nanoseconds as shown in Figure 9.

FIGURE 8 Electronic Resolution and Linearity

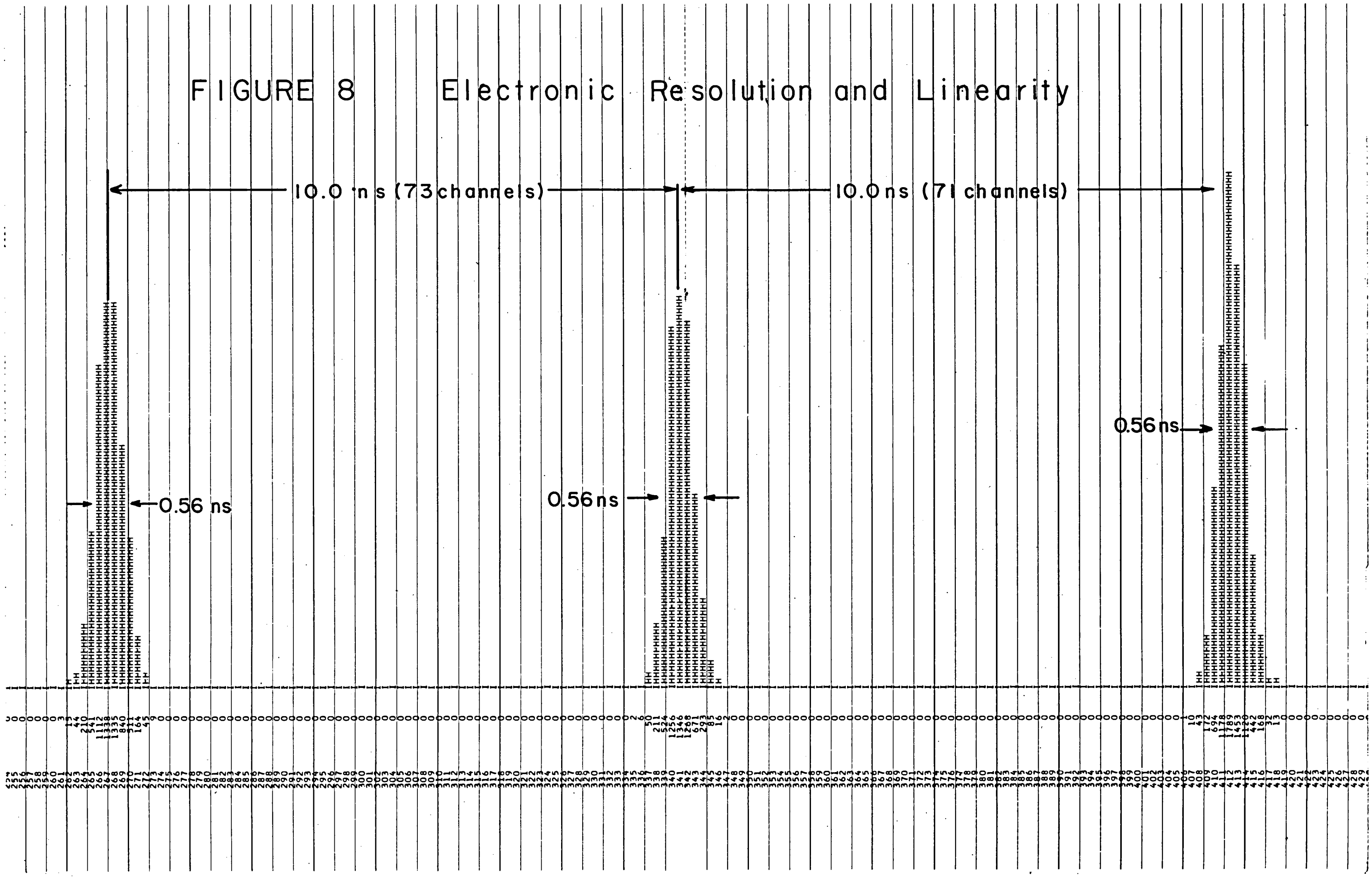

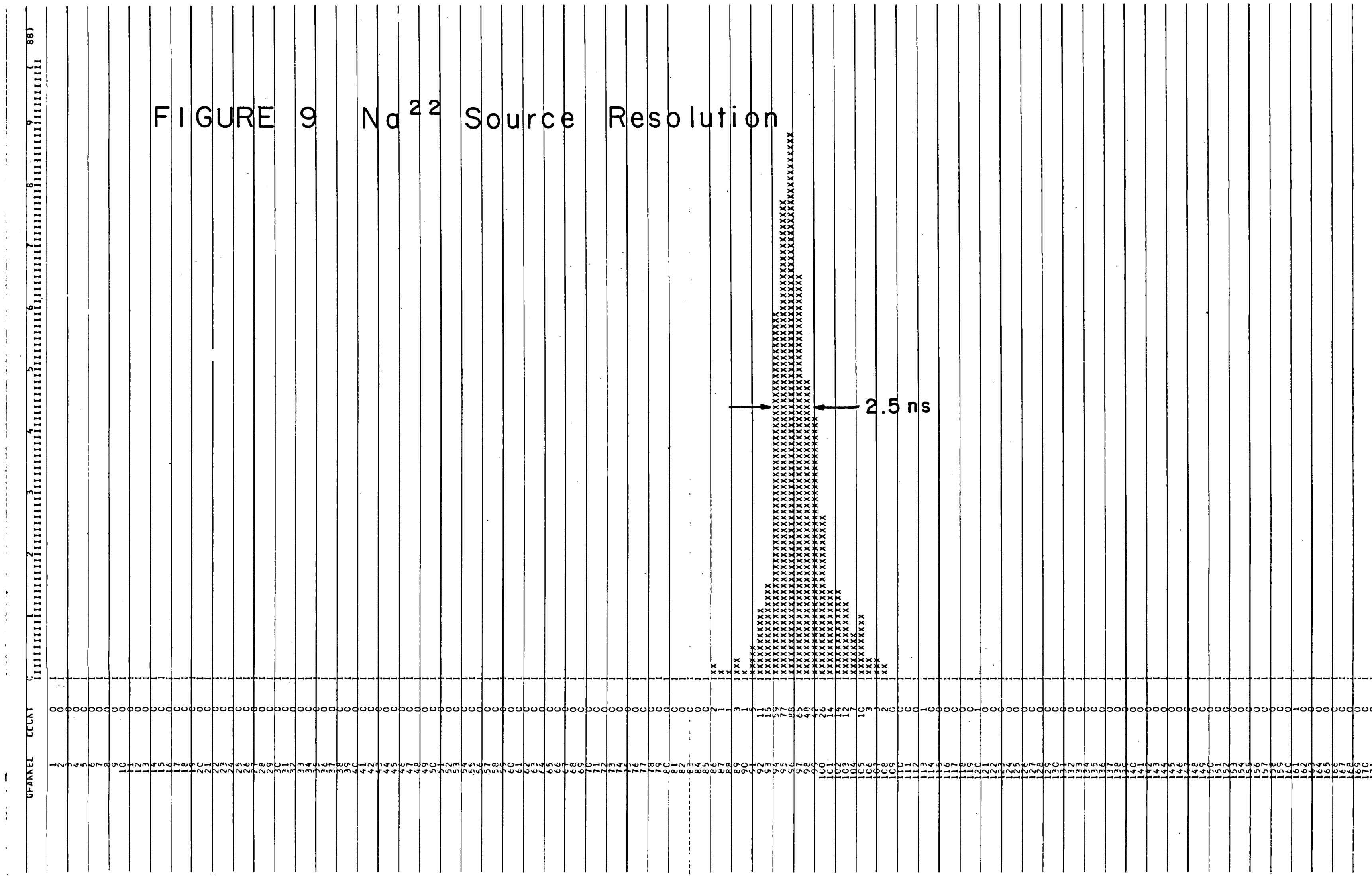

FIGURE 9 Na^{22} Source Resolution

The differential linearity was measured by placing a Co^{60} γ- source between the two scintillators. Instead of the electron-positron annihilation of the Na^{22} source in which only two photons of 0.511MeV appeared in opposite direction, the Co^{60} can decay to either the 2.50 MeV or the 1.33 MeV level of Ni^{60} by beta transitions. The beta decay to the 2.50 MeV level occurs 99.7% of the time and cascade gamma rays of energy 1.17 and 1.33 MeV are emitted in coincidence in the decay to the ground state. These gamma emissions have no preferred spacial orientation however and there is a strong probability that two uncorrelated transitions will trigger the timing event inputs of the time-to-pulse-height converter. The random, statistically constant background offers a measure of the differential linearity which is indicated by Figure 10 to be about twenty percent for the time-of-flight system. The coincident peak of the correlated gamma transitions is shown with a time resolution of about 3.6 nanoseconds. A theoretical calculation by E. Gatti and V. Svelto[6)] results in a possible time resolution of 1.2 nanoseconds for the coincidence of the cascade gamma transition.

FIGURE 10

Co^{60} Source Resolution and Accidental Background

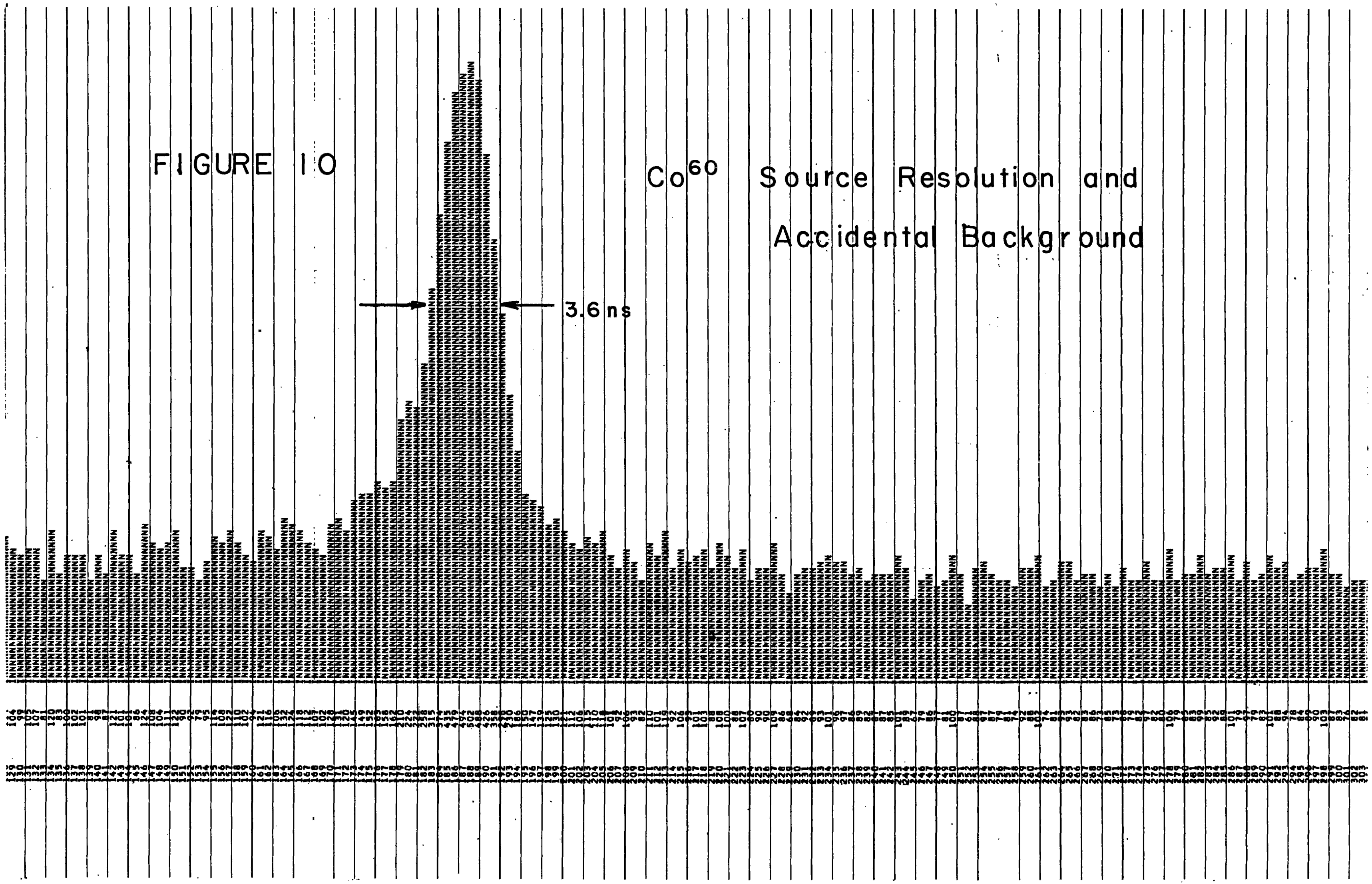

III. EXPERIMENTAL RESULTS

Experimental Configurations

Two experimental configurations were used to obtain data with the time-to-pulse-height converter. The first arrangement is shown in Figure 11 using the associated particle method to observe the monoenergetic neutrons from the first excited state of Li^7 $(p,n'\gamma)$ Be^7 with a proton energy of 3.5 MeV. The first excited state decays to the ground state by gamma ray emission with an energy of 0.43 MeV. This associated gamma ray is detected by a two inch NaI ($T\ell$) scintillator placed about 20 centimeters from the target. Since the counting rate in this counter is high because of its proximity to the target and the high gamma ray flux from background reactions, the output of this photomultiplier tube is delayed by one hundred nanoseconds and connected to the stop event input of the time-to-pulse height converter. In the converter, the stop event input is gated off until a start event input signal is received from the neutron detector. The neutron detector is a plastic scintillator coupled to a fast, high gain photomultiplier tube with its output connected to the start input of the converter. The neutron detector was placed at 90° with respect to the beam at a distance of one-half meter.

Several methods were used in an attempt to reduce the background counting rate. To reduce the sensitivity of the neutron detector to gamma rays, a thin lead shield was placed in front of the plastic scintillator. A slow coincidence requirement was placed on the output of the time-to-pulse-height converter with the output of the tenth dynode of the RCA 6810 photomultiplier tube of the gamma ray detector that was amplified and gated by a single channel analyzer to select only the 0.43 MeV gamma ray transition.

FIGURE II TIME-OF-FLIGHT SYSTEM

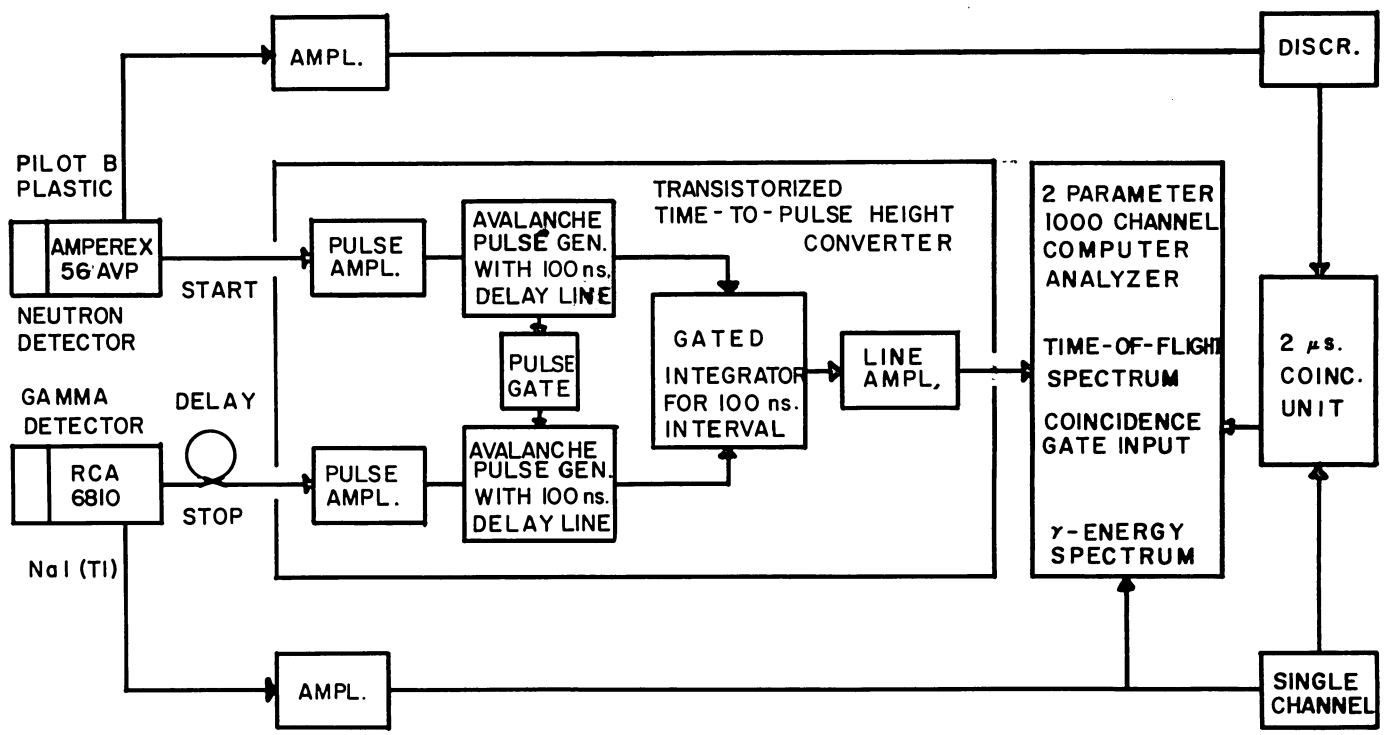

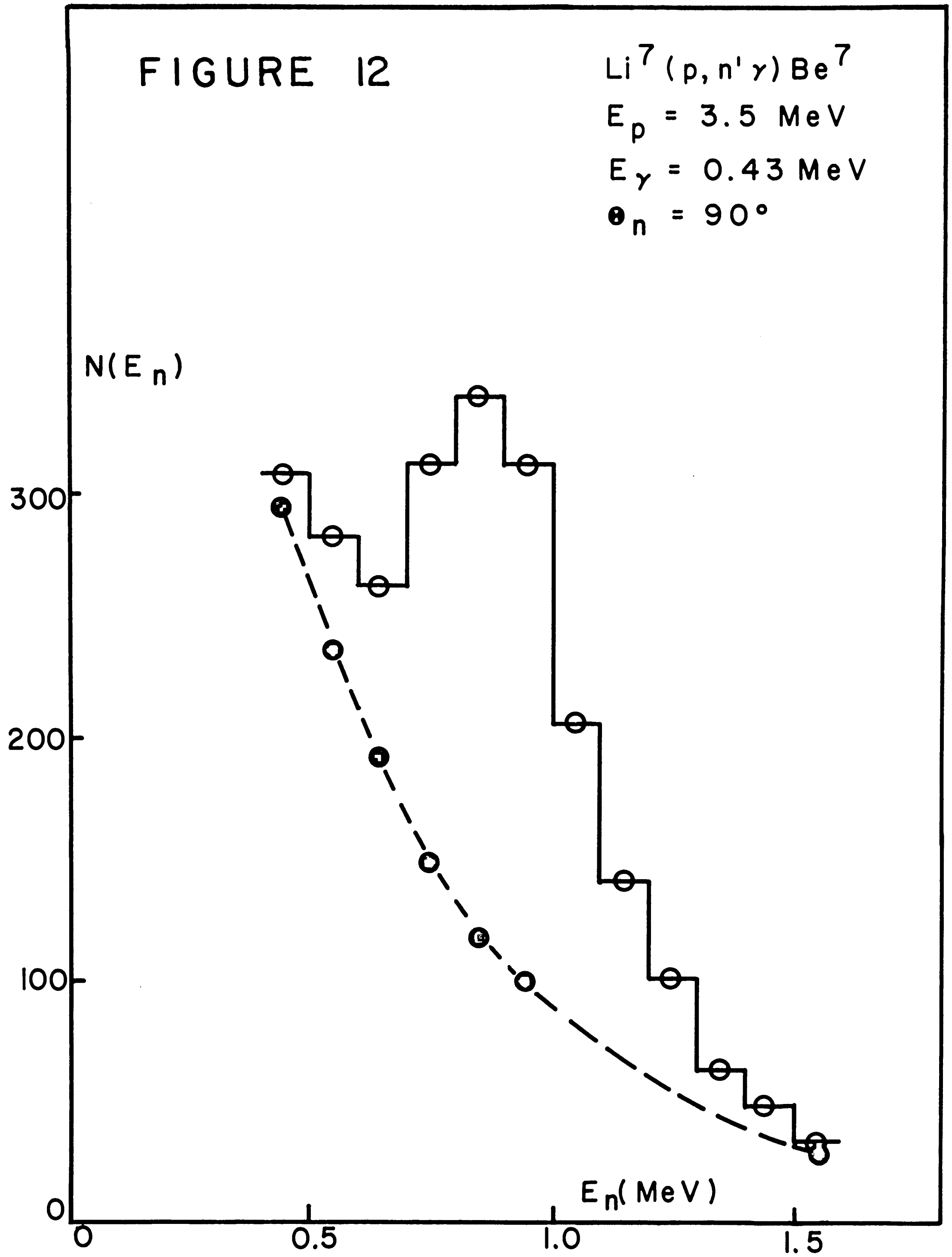

FIGURE 12
Li 7 (p, n' γ) Be 7
E p = 3.5 MeV
E γ = 0.43 MeV
θ n = 90°
N(E n)
300
200
100
0
E n(MeV)
0
0.5
1.0
1.5

In addition to the coincidence requirement of the selected gamma ray energy and the output of the converter, a third requirement was added from the output of the tenth dynode of the neutron detector to discriminate against low level pulses. The third requirement affected the true counting rate to some extent; however, it did reduce the background noticeably and mainly improved the resolution of the neutron peak by preventing an output when the neutron pulse from the scintillator was low enough to cause considerable walk in the timing event discriminators on the input of the time-to-pulse-height converter.

Even with the careful shielding and coincidence requirements, it was impossible to reduce the background low enough to see the neutron peak from the first excited state at a proton energy higher than 3.5 MeV. Figure 12 shows the results of the time of flight measurements at E_p=3.5 MeV of the 0.9 MeV neutron from the target reaction at ninety degrees. The limitations of low neutron yield from target reaction and higher gamma ray background prevented any observation to be made at higher proton energies.

The second configuration shown in Figure 13, was successfully used to observe neutron-proton and neutron-deuteron scattering. In this configuration, two plastic scintillators are used as neutron detectors. Neutrons from the target reaction Li^7 $(p,n'\gamma)$ Be^7 are elastically scattered by the protons of the first plastic scintillator and are detected in the second plastic scintillator. The time interval between the neutron event in the first detector and its arrival at the second detector is measured by the time-to-pulse-height converter to determine the energy of the elastically scattered neutron. As in the first configuration, the signal from the first detector is delayed by a hundred nanoseconds or more

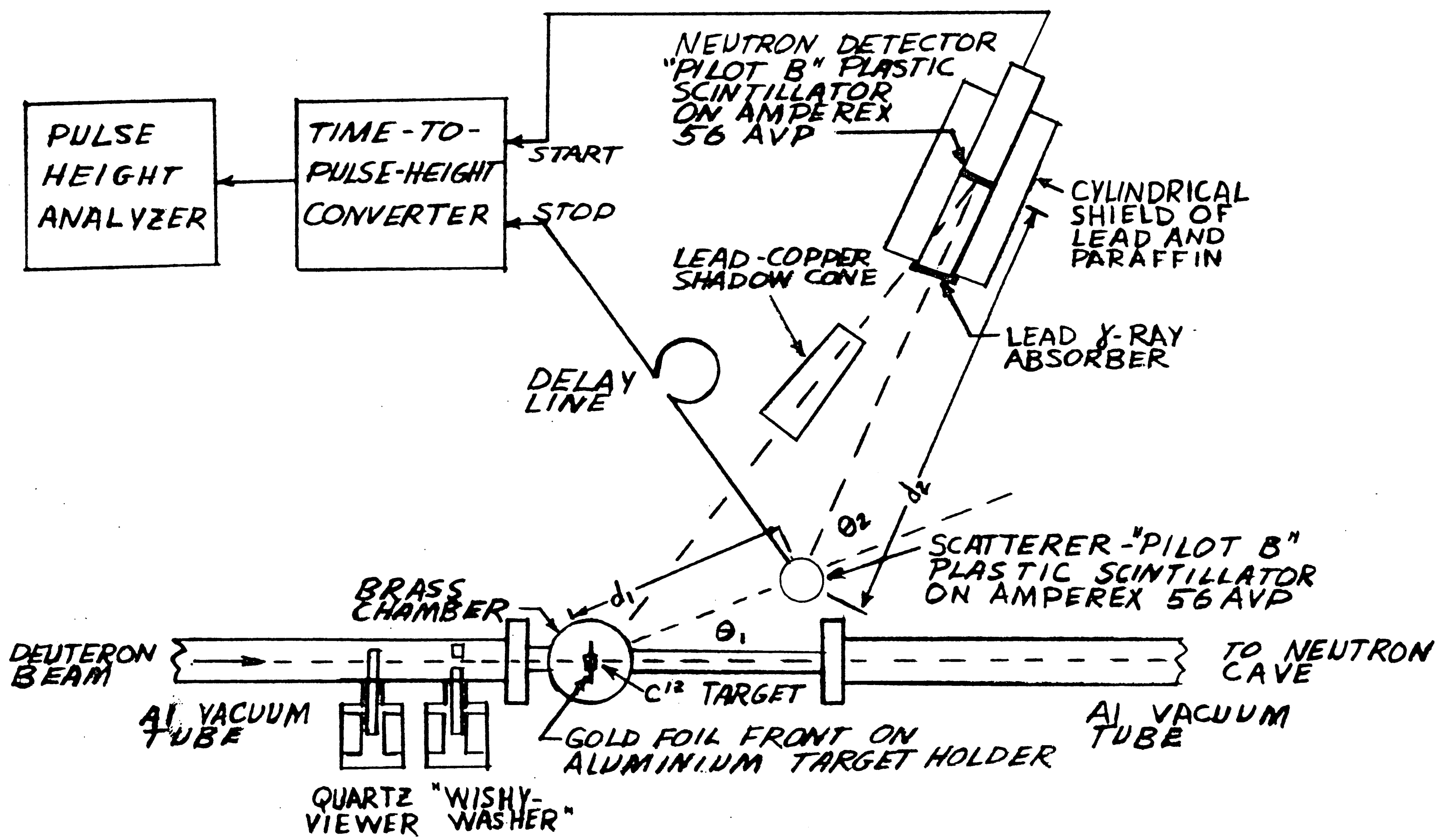

NEUTRON - PROTON SCATTERING EXPERIMENT

FIGURE 13

and connected to the stop event input of the converter since the neutron flux at the first counter is higher than at the second counter. The first detector is the scattering target and the recoil proton whose range is not sufficient to leave the detector produces the scintillation to initiate a stop event pulse from the photomultiplier tube.

The effects of various geometrical arrangements were studied at the first of the experiment to determine the best geometry that produced satisfactory resolution and counting rate with low background. Table I shows the results of various types of shielding that was employed and its effect on the ratio of the time-of-flight peak height to the average background level. The experiment began with completely open geometry. The neutrons were produced by the $C^{12}(d,n)\,N^{13}$ reaction in a brass chamber five feet above a raised aluminum floor. The beam was normally stopped outside the target room approximately thirty feet from the target. A quartz viewer before the target was used to coarsely focus the deuteron beam. A small washer with a quarter-inch hole was then used to finely adjust the beam on the target by obtaining a null with the fringe beam current on the washer. The "wishy-washer" was removed by a solenoid during the course of the experiment; however, it could be inserted at any time to insure that the beam was properly focused on the target.[7] With the open geometry and the distances as shown for run number 7 in Table I, a peak-width resolution of 41% and a peak-to-background ratio of less than 2 was obtained. The peak-to-background ratio was improved to over 4 in run number 8 by placing the second detector in a large shield of lead and lithium-loaded paraffin. Run number 10 shows some degradation in the resolution at a large angle due to the larger variations in energy of the elastically scattered neutron with angular spread since the energy varies as the cosine squared.

TABLE I

INITIAL SET-UP AND SHIELDING

Run No.	E_n	d_1	d_2	Θ_1	Θ_2	E_n scatt.	E_n exp.	ΔE_n	%ΔE	Peak/Bkgd.	Remarks
	MeV	cm	cm			MeV	MeV	MeV			
7	3.63	25	75	13°	30°	2.72	2.95	1.2	41%	1.92	Open geometry
8	3.63	25	75	13°	30°	2.72	2.60	1.3	50%	4.20	Shielded counter #2
10	3.63	25	75	13°	50°	1.49	0.95	0.7	74%	2.70	Shielded counter #2
11	3.63	25	75	13°	50°	1.49	1.05	0.6	57%	3.20	Shadow cone added
15	3.54	25	75	30°	50°	1.46	1.55	0.9	58%	10.1	Gold around target holder

A shadow cone of iron was added between the target and the second detector in run number 11 which tended to improve the peak-to-background ratio compared with run number 10. The best geometrical arrangement was decided uponin run number 15 with the gold-foil stopping the beam near the target removed, the shadow cone in place, the second detector shielded with a thin lead absorber for gamma rays over the front of the entrance to the shield, and a gold-foil facing on the aluminum target holder around the carbon target. A peak-to-background ratio of ten was achieved.

Table II shows the expected appearance of the second neutron group from the carbon 12 target reaction at higher deuteron energies. Run numbers 18, 19, and 30 give the observed scattered neutron energies with the observed resolutions and peak-to-background ratios for beam energies of E_d=4,5, and 6 MeV respectively. Run number 30 also illustrates the rapid increase of background at beam energies greater than 5 MeV. The resolution of the time-to-flight peak is improved by the greater distance of the initial scatterer from the target and the longer flight path. This improvement indicates the amount of variation in scattered neutron energy solely due to angular spread and thickness of the scintillation crystals. The effect of improving the peak-to-background ratio slightly by a new target is shown in Table III with a beam energy of E_d = 5 MeV. The improved resolution with a smaller solid angle subtended by the initial scatterer is again illustrated in the results of run number 23.

Table IV shows the results of run number 57 and 58 during which the plastic scintillator used as the initial scatterer was made smaller to give less angular spread. In run number 59, the smaller scatterer was placed closer to the target and only a slight improvement in resolution was noted with this small change in volume and solid angle. In fact, the

TABLE II

CHANGE OF BEAM ENERGY, E_d = 4, 5, AND 6 MeV

Run No.	E_n	d_1	d_2	Θ_1	Θ_2	E_n scatt.	E_n exp.	ΔE_n	%ΔE	Peak/Bkgd.	Remarks
	MeV	cm	cm			MeV	MeV	MeV			
18	3.54	25	75	30°	39°	2.12	2.25	1.4	62%	17.5	E_d = 4 MeV (Only one state)
19 (gnd state)	4.50	25	75	30°	39°	2.70	2.65	1.4	53%	18.4	E_d = 5 MeV (Two states appear)
19 (1st state)	2.02	25	75	30°	39°	1.22	1.25	0.6	48%	8.4	E_d = 5 MeV
30 (gnd state)	5.45	50	129.5	30°	38°	3.38	3.35	1.1	33%	2.3	E_d = 6 MeV (higher bkgd)
30 (1st state)	3.0	50	129.5	30°	38°	1.86	1.80	0.7	40%	2.6	E_d = 6 MeV

TABLE III

CHANGE TO NEW TARGET AND MOVE SCATTERER AWAY

Run No.	E_n MeV	d_1 cm	d_2 cm	Θ_1	Θ_2	E_n scatt. MeV	E_n exp. MeV	ΔE_n MeV	%ΔE	Peak/Bkgd.	Remarks
21 (gnd state)	4.5	25	75	30°	52°	1.71	1.55	1.1	71%	4.4	Old target
21 (1st state)	2.02	25	75	30°	52°	0.77	0.84	0.6	71%	2.6	E_d = 5 MeV
22 (gnd state)	4.5	25	75	30°	52°	1.71	1.55	1.0	64%	5.4	Thicker target
22 (1st state)	2.02	25	75	30°	52°	0.77	0.80	0.5	63%	3.0	E_d = 5 MeV
23 (gnd state)	4.5	50	75	30°	50°	1.84	1.65	0.7	42%	10.0	Smaller solid angle
23 (1st state)	2.02	50	75	30°	50°	0.83	0.80	0.4	50%	5.0	

TABLE IV

EFFECT OF SMALLER SCATTERER

Run No.	E_n MeV	d_1 cm	d_2 cm	Θ_1	Θ_2	$E_{n\ scatt.}$ MeV	$E_{n\ exp.}$ MeV	ΔE_n MeV	%ΔE	Peak/Bkgd.	Remarks
57	3.54	50	75	30°	40°	2.07	2.05	0.8	39%	7.1	5 x 3.5 cm. scatterer size
58	3.54	50	75	30°	40°	2.07	2.25	0.8	36%	5.4	5 x 2 cm. scatterer size
59	3.54	22	75	30°	40°	2.07	2.20	0.8	37%	6.4	5 x 2 cm. scatterer size

smaller volume tended to cause a slight increase in background due to the lower probability of collision and scintillation in the smaller volume. The fact that the second detector for the scattered neutrons consisted of a 5 centimeter thick crystal throughout which a scintillation may occur at any point caused approximately a 10% error in the measurement of the time interval over the flight path of 75 centimeters when combined with the diameterof the initial scatterer which was a plastic crystal 3.5 centimeters in diameter for run number 57 and 2.0 centimeters for run numbers 58 and 59. Therefore, over one-half of the resolution of the peak half-width may be assigned to variations in energy due to both angular spreads and flight paths. The amount of spread due to walk in the trigger point in the electronics over a 10:1 pulse height range is estimated from these experimental runs to be less than 3 nanoseconds as was previously determined by the source calibrations. Out of the flight time of 31 nanoseconds for the 2 MeV neutrons over the 75 centimeter path, a time spread of less than 10% or an energy spread of less than 20% was caused by the time-to-pulse height converter.

Angular Distribution For *n,p* Scattering

To evaluate the efficiency of the time-of-flight system, the second experimental arrangement was used to measure neutron yields from *n,p* scattering at incident neutron energies of 3.5 and 4.5 MeV. The incident neutrons were produced by the C^{12} (d,n) N^{13} reaction with the plastic scintillator scatterer at 30° from the 4 or 5 MeV deuteron beam. Three set runs of angular distributions were measured at angles between 25° and 60° with the neutron detector 100 centimeters from the scatterer. In the first two set runs, a cylindrical plastic scatterer 4.5 cm. in diameter by 5 cm. height was placed 50 cm. from the target with the axis of the cylinder perpendicular to the incident neutron flux. The cylindrical neutron detector was 4.5 cm. in diameter by 5 cm. thick with its axis parallel to the scattered neutron flux. In the third set run, the scatterer size was reduced to 1.27 cm. diameter by 1.27 cm. high and placed 15 cm. from the target while the thickness of the neutron detector was reduced to 2.5 cm. The deuteron beam energy of the first and third set runs was 4 MeV producing a 3.5 MeV incident neutron flux on the scatterer while the second set run used a 5 MeV deuteron beam to produce an incident neutron flux of 4.5 MeV. As previously described, the scintillation from the recoil proton in the scatterer was used to generate the stop event signal which was delayed approximately 80 nanoseconds before connection to the converter while the neutron detector generated the start event signal. With this arrangement, the yield was expected not only to vary with scattered neutron energy, but also with the energy of recoil proton.

Figure 14 shows the typical experimental time spectrum at a scattering angle of 54° for the three set runs. The scattered neutron energy is 1.23 MeV for the data shown of run number 114. The time zero is located to the left side of the figure as indicated by the prompt gamma peak from correlated gamma transitions of background reactions. The time calibration is 0.47 nanosecond per channel. This set run also included a deuterated Benzene scintillator mounted on top of the plastic scatterer to compare the results of n,p scattering with n,d scattering. The comparison is shown only to illustrate the time resolution of n,d experiments. The pulse heights from the deuterated Benzene scintillator are not identical and a comparison of relative yields can not be made.

FIGURE 14 Run Number 114 Time Spectrum

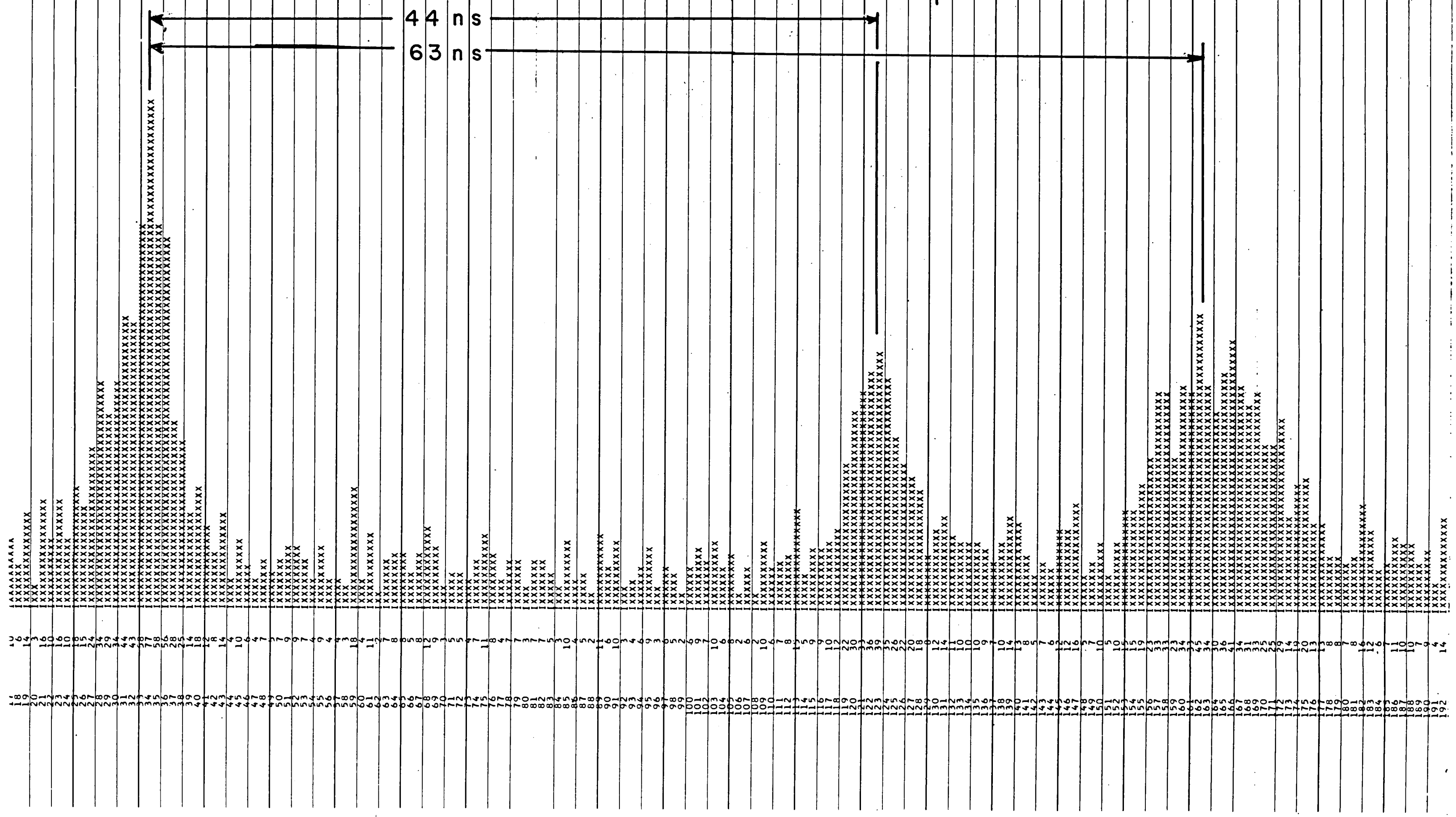

After the experimental runs were completed, the energy spectrums were computed and printed by the IBM 1401 from the data of the time spectrum which had been sequenced to the computer and stored on magnetic tape. The computed energy spectrum for run number 114 at an angle of 54° is shown in Figure 15. The computer program automatically subtracts the average background counts before computing the energy spectrum. Table 10 and 11 shows the complete results of the set runs for all angles taken between 25° and 60°. Run numbers 36 thru 39 were assigned to the first set run, 43 thru 47 to the second set run and 106, 108, 110, 114, 115 and 117 were chosen as representative *n,p* and *n,d* scattering data from the third set run. In the tables the yield is indicated first as the total number of counts accumulated in the neutron peak minus the average background counts. Then the yield was normalized to one millicoulomb of deuteron beam current to facilitate the calculation of the efficiency of the neutron detector.

Efficiency Of The Time-Of-Flight System

The experimental yields obtained in the three set runs were compared with calculated yields obtained from the known values of the *n,p* scattering cross-section. Table V shows the calculation to arrive at the number of neutrons per steradian incident on the plastic scatterer placed at 30° from the target axis for one millicoulomb beam. The carbon target was approximately 0.48 milligrams per square centimeter thick and 20 millibarns per steradian was taken for the cross-section of the target reaction[9]. The solid angles subtended by the two sizes of scatterers are shown in Table VI.

FIGURE 15

Run Number 114

Energy Spectrum

ENERGY	YIELD	INTEGYIELD
0.5500	-1.07600	-1.07600
0.6500	-0.22960	-1.30600
0.7500	-0.11580	-1.42200
0.8500	0.00520	-1.41700
0.9500	0.13170	-1.28500
1.0500	0.21790	-1.06700
1.1500	0.88080	-0.18620
1.2500	1.68100	1.49500
1.3500	1.67400	3.16900
1.4500	1.19900	4.36800
1.5500	0.44910	4.81700
1.6500	0.03540	4.85200
1.7500	0.16070	5.01300
1.8500	0.02090	5.03400
1.9500	0.09420	5.12800
2.0500	0.10840	5.23600
2.1500	0.07060	5.30700
2.2500	0.10670	5.41400
2.3500	0.16290	5.57700
2.4500	0.17900	5.75600
2.5500	0.38010	6.13600
2.6500	0.30420	6.44000
2.7500	0.80830	7.24800
2.8500	0.70150	7.95000
2.9500	0.39340	8.34300
3.0500	0.27160	8.61500
3.1500	0.05860	8.67400
3.2500	0.02970	8.70400
3.3500	0.00180	8.70600
3.4500	-0.00520	8.70100
3.5500	0.06680	8.76800
3.6500	0.00500	8.77300
3.7500	-0.00610	8.76700
3.8500	0.00900	8.77600
3.9500	-0.01100	8.76500
4.0500	-0.02990	8.73500
4.1500	-0.02190	8.71300
4.2500	-0.03390	8.67900
4.3500	0.00610	8.68500
4.4500	-0.00880	8.67600
4.5500	0.01920	8.69500
4.6500	0.00830	8.70300
4.7500	0.00320	8.70600
4.8500	0.01330	8.71900
[illegible]	-0.00470	8.71400

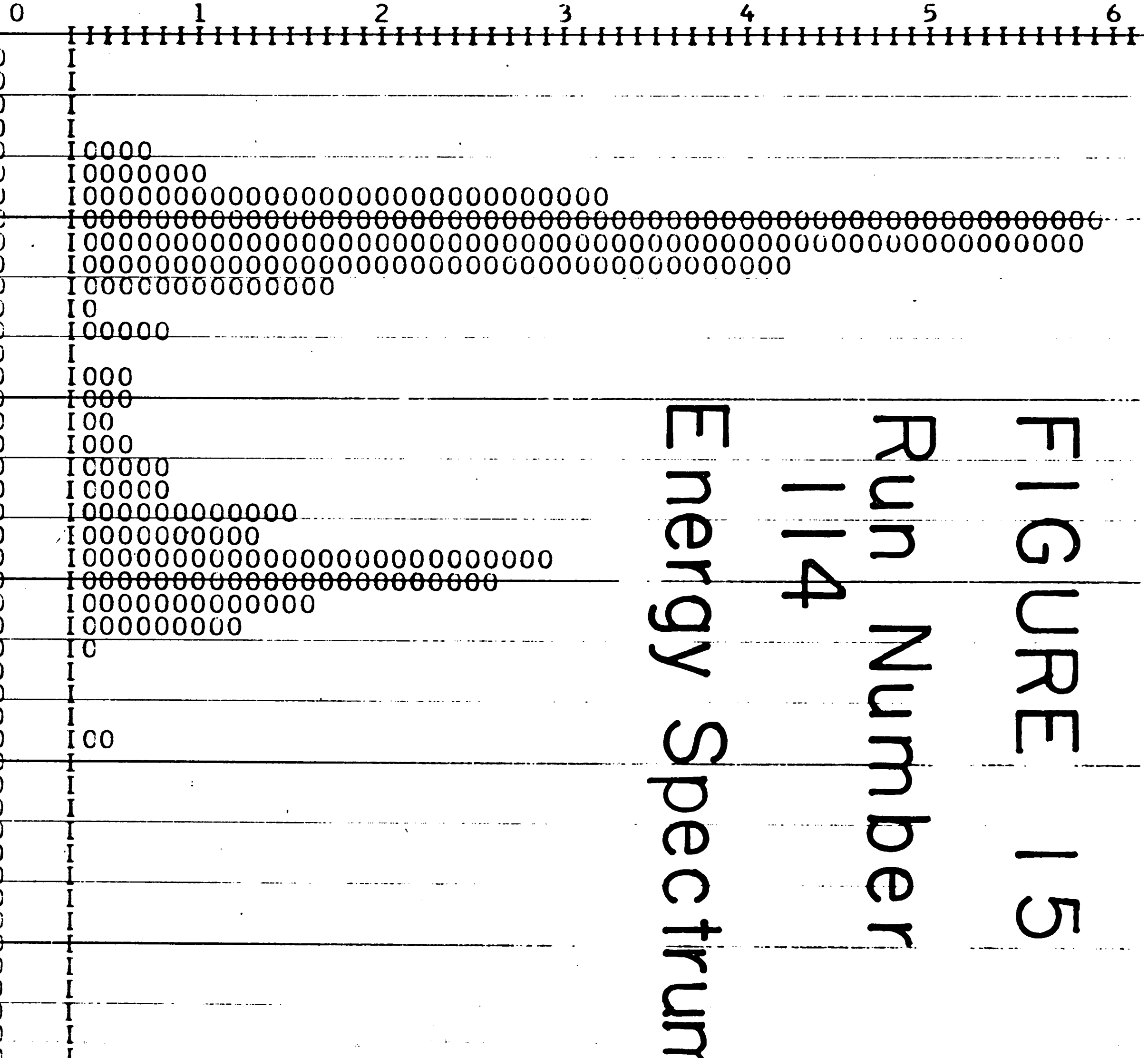

The number of scattering centers in the two plastic scintillators are calculated in Table VII. The density of the plastic was 1.05 grams per cubic centimeter. The equivalent gram molecular weight was found from information on the data sheet of the Pilot "B" plastic giving the ratio of hydrogen atoms to carbon atoms as 1.1. The solid angle subtended by the neutron detector was the same for all runs and is shown in Table VIII.

The cross section for n,p scattering is isotropic in the center of mass. For incident neutron energy of 3.5 MeV the total cross section is 2.2 barns. For incident neutron energy of 4.5 MeV, the total cross section is 1.8 barns. The differential cross section for the laboratory system of coordinates is calculated from the equation[10]:

$$\partial\sigma/\partial\Omega = (\sigma_T \cos\theta) \;/\; \pi$$

Table IX shows the calculated results at the angles used in the three set runs.

From the numbers tabulated in Tables V, VI, VII, VIII, and IX, the expected neutron yield per millicoulomb of beam is calculated and shown in Table X. Comparing the experimental yield with the calculated yield indicates the efficiency of the neutron detection system. The resulting efficiencies are listed in Table X and plotted in Figure 16.

Apparent in the plot of the efficiency of the time of flight system is the decrease in efficiency with the energy of the recoil proton. This variation would not be present if a pulsed-beam were used as the delayed stop signal, however in the present experiment the threshold of the stop signal was about 1.5 MeV in the first and second runs and less than 1.0 MeV in the third run. The thresholds for the neutron detector were approximately

TABLE V

NUMBER OF NEUTRONS INCIDENT ON SCATTERER PER STERADIAN AT 30° FROM

$C^{12}(d,n)N^{13}$ PER MILLICOULOMB DEUTRON BEAM

N_n = 0.625 x 10^{19}(deuterons/coulomb) x 10^{-3}(coulombs/millicoulomb)

x 0.48(milligrams/cm^2) *target thickness* x 6 x 10^{23}(atoms/gm atomic wt.)

x 1/12(gms/gm atomic wt.) x 10^{-3}(gms/milligram)

x 20 x 10^{-27}(cm^2/steradian) *target yield at 30°, 4 to 5 MeV*

= 3.0 x 10^9(neutrons at 30° / steradian-millicoulomb beam)

TABLE VI

SOLID ANGLE OF SCINTILLATOR USED AS SCATTERER

Scatterer Size	Area of Scatterer cm^2	Distance to Target cm	Solid Angle steradian
4.5 cm diameter by 5 cm high	22.5	50.0	9×10^{-3}
1/2 in. diameter by 1/2 in. high	1.61	15.0	7.16×10^{-3}

TABLE VII

NUMBER OF PROTONS IN CH SCATTERER PER SQUARE CENTIMETER

For 4.5 x 5 cm Scatterer:

$$N_p = \pi \times (4.5/2)^2\ (\mathrm{cm}^2) \times 5(\mathrm{cm}) \times 1.05(\mathrm{gm/cm}^3) \times 6 \times 10^{23}\ (\text{H atoms/gm equivalent molecular weight})$$

$$\times\ 1/11.9(\text{gms/gm equivalent molecular weight}) \times 1/4.5 \times 5(\mathrm{cm}^2)$$

$$= 1.87 \times 10^{23}\ (\mathrm{protons/cm}^2)$$

For 1/2 x 1/2 in. Scatterer:

$$N_p = \pi \times (1.27/2)^2\ (\mathrm{cm}^2) \times 1.27(\mathrm{cm}) \times 1.05(\mathrm{gm/cm}^3) \times 6 \times 10^{23}\ (\text{H atoms/gm equivalent molecular weight})$$

$$\times\ 1/11.9(\text{gms/gm molecular weight}) \times 1/1.27 \times 1.27(\mathrm{cm}^2)$$

$$= 5.28 \times 10^{22}\ (\mathrm{protons/cm}^2)$$

TABLE VIII

SOLID ANGLE OF NEUTRON COUNTER

Detector Size	Area of Detector cm^2	Distance from Scatterer cm	Solid Angle steradian
4.5 cm diameter	15.9	100	1.59×10^{-3}

TABLE IX

DIFFERENTIAL CROSS-SECTIONS FOR NEUTRON-PROTON SCATTERERING

	For Incident Neutron Energy = 3.5 MeV:	For Incident Neutron Energy = 4.5 MeV:
Scattering Angle degrees	Differential Cross-section 10^{-24} cm^2/steradian	Differential Cross-section 10^{-24} cm^2/steradian
25	-----	0.520
30	0.606	0.496
33	0.586	-----
38	0.551	-----
40	0.536	0.438
44	0.504	-----
50	0.450	0.368
54	0.411	-----
60	0.350	0.286

TABLE X

EFFICIENCY VS SCATTERED NEUTRON ENERGY FOR TIME-OF-FLIGHT SYSTEM

Size of Scatterer = 4.5 cm diameter by 5 cm height

Size of Detector = 4.5 cm diameter by 5 cm thick

Target to Scatterer Distance = 50 cm.

Scatterer to Detector Distance = 100 cm.

Average Energy Resolution = 36%

Run No.	$E_n^{incid.}$ MeV	$\theta^{scatt.}$ degrees	$E_n^{scatt.}$ MeV	E_p^{recoil} MeV	Counts in Peak minus Backgnd.	Integ Beam mcoul.	Norm. Yield to 1 mcoul.	Calc. Yield for 1 mcoul.	Eff. %
39	3.54	60	0.89	2.65	580	1.93	300	2810	10.7
43	4.50	60	1.13	3.37	544	2.03	268	2296	11.7
38	3.54	50	1.45	2.09	1182	1.93	612	3613	16.9
44	4.50	50	1.87	2.63	1177	1.93	606	2954	20.5
37	3.54	40	2.07	1.47	1182	1.93	613	4303	14.2
45	4.50	40	2.63	1.85	1352	1.93	700	3516	19.9
36	3.54	30	2.65	0.89	767	1.93	397	4865	8.2
46	4.50	30	3.38	1.12	912	2.03	450	3982	11.3
47	4.50	25	3.69	0.81	552	1.93	286	4175	6.9

TABLE XI

EFFICIENCY VS SCATTERED NEUTRON ENERGY FOR TIME-OF-FLIGHT SYSTEM

Size of Scatterer = 1/2 in. diameter by 1/2 in. height

Size of Detector = 4.5 cm diameter by 2.5 cm thick

Target to Scatterer Distance = 15 cm.

Scatterer to Detector Distance = 100 cm.

Average Energy Resolution = 28%

Run No.	$E_n^{incid.}$ MeV	$\theta^{scatt.}$ degrees	$E_n^{scatt.}$ MeV	E_p^{recoil} MeV	Counts in Peak minus Backgnd.	Integ Beam mcoul.	Norm. Yield to 1 mcoul.	Calc. Yield for 1 mcoul.	Eff. %
110	3.54	60	0.89	2.65	336	8.25	40	631	6.5
114	3.54	54	1.23	2.31	510	4.06	125	741	16.9
108	3.54	50	1.45	2.09	634	5.18	122	811	15.0
106	3.54	44	1.81	1.73	524	4.06	129	909	14.2
117	3.54	38	2.20	1.35	926	6.10	152	993	15.3
115	3.54	33	2.50	1.04	700	4.06	172	1057	16.3

the same as the recoil proton. For the first and second set runs, the threshold sensitivity was about 1 volt. For the third set run, the input sensitivity was improved to 0.5 volt discrimination level. The difference between the first and second runs is illustrated by the extension of the maximum efficiency by 1 MeV corresponding to the 1 MeV increase in incident neutron energy and the resulting increase in recoil proton energy. The efficiency of the neutron detector at energies of the scattered neutron less than 1.5 MeV was unchanged by the incident neutron energy and the efficiency decreases identically for the first and second set runs.

The efficiency of the third set run would appear to be one-half that of the first two runs because the scintillator used for the neutron detector was reduced to one-half thickness. However, this was compensated by the lower threshold sensitivity of the converter which improved the efficiency by increasing the response of the system to both neutrons and recoil protons of lower energy. The experimental efficiencies for the three set runs assumes that each time a neutron is scattered at the angle of the neutron detector, the recoil proton in the scatterer produces a scintillation which causes a stop event signal in the time-to-pulse height converter.

It is possible to calculate the maximum efficiency of the organic scintillator from the number of hydrogen atoms per square centimeter in the scintillator and the *n,p* scattering cross section in which the empirical value in the neighborhood of 1 MeV for the cross section is[11)]

$$\sigma_{(E)} = (4.83 / \sqrt{E_{inc.}\ \mathrm{MeV}}) - 0.578 \text{ barns}$$

Then the maximum efficiency for an incident neutron energy of 2 MeV with the scintillator of the first two set runs is

$$\text{Eff.}_{(2\ \text{MeV})} = 1.87 \times 10^{23}\ (\text{Protons} / \text{cm}^2) \times 2.84 \times 10^{-24}\ \text{cm}^2 = 53\%$$

For the third set run, the maximum efficiency would be one-half because the scintillator thickness was reduced by one-half.

To find the actual efficiency of the neutron detector the threshold energy of the system must be considered. Therefore it is necessary to reduce the maximum efficiency by the factor $(1 - B / E)$ where B is the bias energy and E is the incident neutron energy. Table XII indicates the calculated efficiency of the neutron detector for the experimental neutron energies and the results are plotted in Figure 16 with the experimental efficiency. The decrease in efficiency with proton recoil energy in the scatterer must be treated similarly and the two threshold factors are multiplied together. For the best fit of the calculated efficiency curve to the experimental results, the threshold energy for the neutron detector was 0.83 MeV and 0.70 MeV for the proton recoil threshold for the first two set runs. For the third set run, the threshold levels were lower, and for the best fit of the calculated efficiency to the experimental results, the threshold energy for the neutron detector was 0.70 MeV and 0.25 MeV for the proton recoil. The calculated values of the thresholds were the same that was expected from observations during the experiment. The experiment and calculated curves were in fairly good agreement.

The factor (1 - B / E) is suitable for calculating the reduction of the maximum efficiency due to the threshold level of the neutron detector discriminator because the output pulses from the photomultiplier tube vary from the incident neutron energy height down to zero energy of the recoil proton. Its corresponding pulse height distribution is rectangular. However in the scintillator used as the scatterer, the proton recoil has a fixed energy of recoil for a given angle of the neutron detector. Therefore, the output pulses from the photomultiplier tube vary according to the resolution of the recoil detection system for recording a neutron-proton scattering event. The shape of the pulse height distribution of the recoil proton output pulse depends on the scattering angle resolution, the scintillator energy resolution, the photomultiplier tube noise, and other variations in the discriminator system. This pulse height distribution is generally Gaussian in shape instead of rectangular as was approximated in the calculation of the efficiency curve. The Gaussian distribution would result in a calculated efficiency curve with a flatter top and a sharper cutoff at the higher neutron energy. The resolution of the experimental data was not good enough to require a more accurate approximation than the assumed rectangular distribution. However, the experimental efficiency curve of Figure 17 does indicate a flatter top with a sharper cutoff than the calculated curve. This resulted from some improvement in the resolution of the data obtained in set runs numbered 106 through 115.

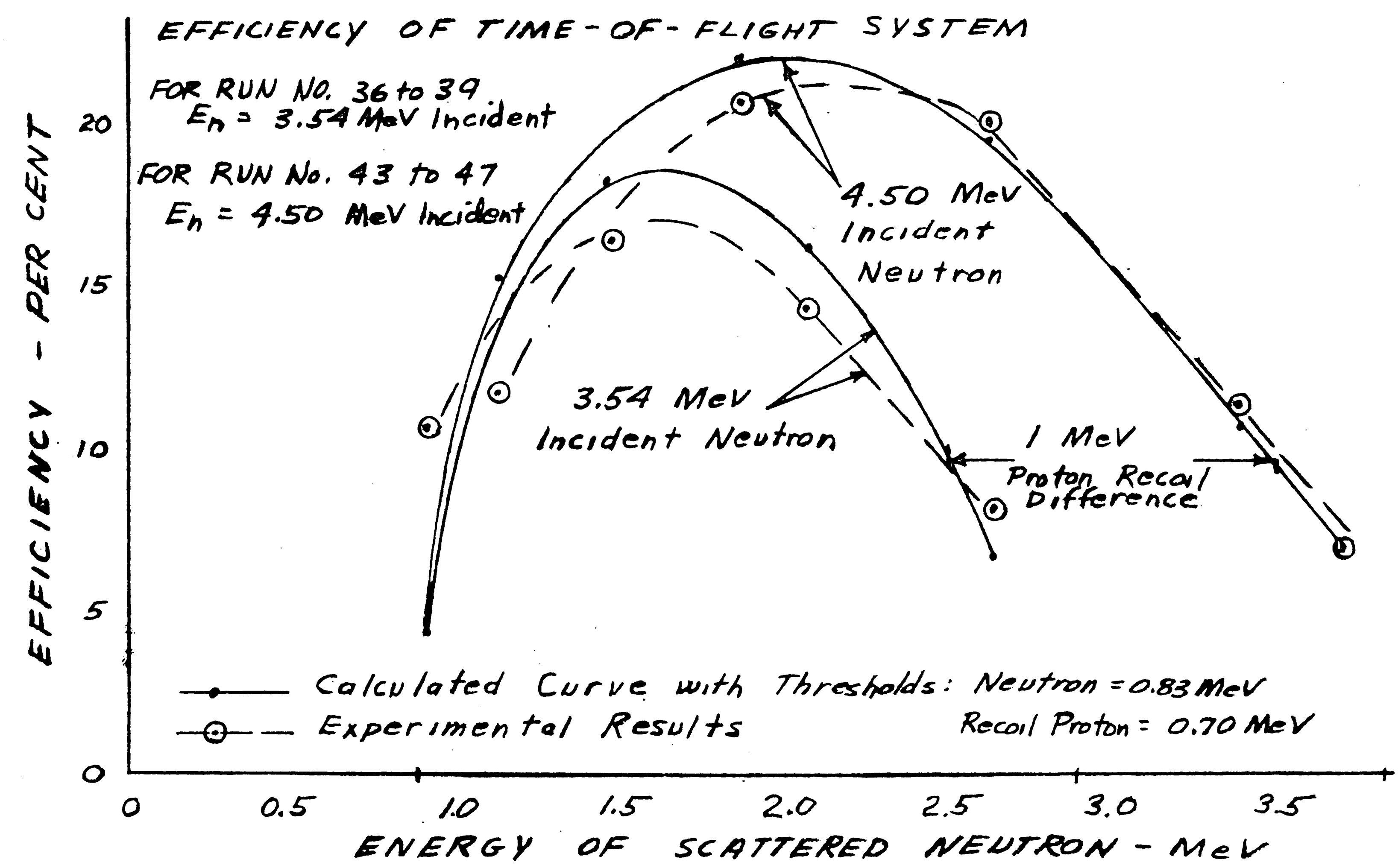
EFFICIENCY OF TIME-OF-FLIGHT SYSTEM
FOR RUN NO. 36 to 39
E_n = 3.54 MeV Incident
FOR RUN No. 43 to 47
E_n = 4.50 MeV Incident
4.50 MeV Incident Neutron
3.54 MeV Incident Neutron
1 MeV Proton Recoil Difference
Calculated Curve with Thresholds: Neutron = 0.83 MeV
Experimental Results
Recoil Proton = 0.70 MeV
EFFICIENCY - PER CENT
0
5
10
15
20
0
0.5
1.0
1.5
2.0
2.5
3.0
3.5
ENERGY OF SCATTERED NEUTRON - MeV

FIGURE 16

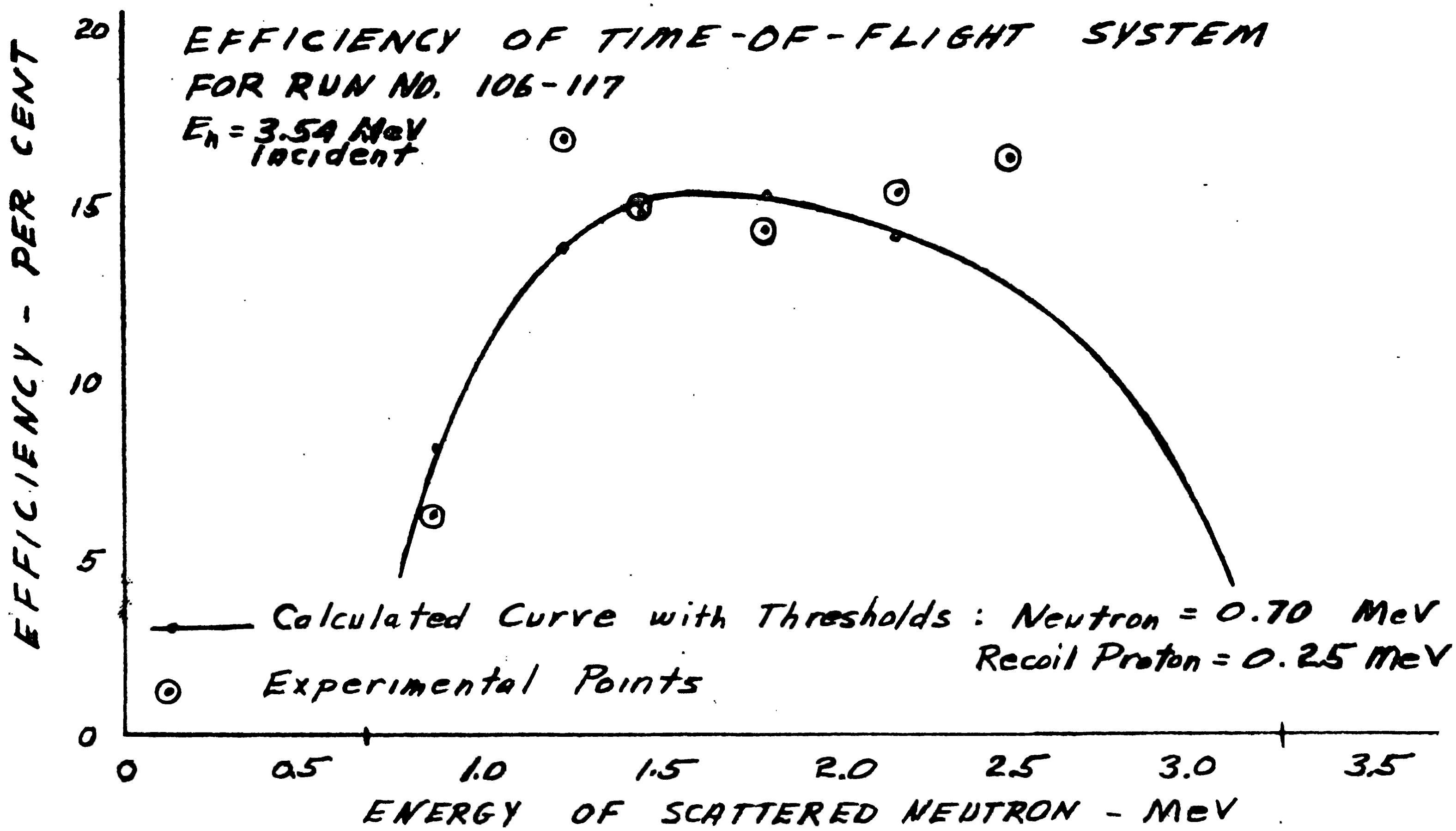
EFFICIENCY OF TIME-OF-FLIGHT SYSTEM
FOR RUN NO. 106-117
E_n = 3.54 MeV Incident
Calculated Curve with Thresholds : Neutron = 0.70 MeV
Recoil Proton = 0.25 MeV
Experimental Points
EFFICIENCY - PER CENT
20
15
10
5
0
0
0.5
1.0
1.5
2.0
2.5
3.0
3.5
ENERGY OF SCATTERED NEUTRON - MeV

FIGURE 17

TABLE XII (a)

CALCULATED EFFICIENCY OF TIME-OF-FLIGHT SYSTEM

N_p = 1.87 x 10^{23}

B_n = 0.83 MeV

B_p = 0.70 MeV

Run No.	E_n MeV	$\sigma_{(E)}$ barns	Eff_{max} %	E_p MeV	$(1-B_p/E_p)$	$(1-B_n/E_n)$	$Eff_{calc.}$ %
39	0.89	4.54	84.8	2.65	.74	.07	4.4
43	1.13	3.96	74.0	3.37	.79	.26	15.2
38	1.45	3.43	64.1	2.09	.66	.42	17.8
44	1.87	2.95	55.1	2.63	.73	.55	22.1
37	2.07	2.77	51.8	1.47	.52	.60	16.1
45	2.63	2.40	44.8	1.85	.62	.69	19.2
36	2.65	2.40	44.8	0.89	.21	.69	6.5
46	3.38	2.04	38.2	1.12	.37	.76	10.8
47	3.69	1.94	36.3	.81	.14	.78	4.0

TABLE XII (b)

CALCULATED EFFICIENCY OF TIME-OF-FLIGHT SYSTEM

$N_p = .94 \times 10^{23}$

$B_n = .70$

$B_p = .25$

Run No.	E_n MeV	$\sigma(E)$ barns	Eff_{max} %	E_p MeV	$(1-B_p/E_p)$	$(1\ B_n/E_n)$	$Eff_{calc.}$ %
110	0.89	4.54	42.6	2.65	.91	.21	8.1
114	1.23	3.78	35.5	2.31	.90	.43	13.7
108	1.45	3.43	32.2	2.09	.88	.52	14.8
106	1.81	3.01	28.3	1.73	.86	.62	15.1
117	2.20	2.69	25.3	1.35	.82	.68	14.1
115	2.50	2.48	23.3	1.04	.76	.72	12.8

IV. REFERENCES

1. G. C. Bonazzola and E. Chiavassa, Nuclear Instruments and Methods 27 (1964) 41-44.

2. P. Huber, Z. Lewandowski, R. Plattner, C. Poppelbaum and R. Wagner, Nuclear Instruments and Methods 14 (1961) 131-137.

3. R. L. Chase, Review of Scientific Instruments 31 No. 9 (1960) 945.

4. S. G. Buccino, C. E. Hollandworth and P. R. Bevington, Nuclear Physics 53 (1964) 375-384.

5. L. P. Hunter ed., Handbook of Semiconductor Electronics 2nd Ed., (McGraw-Hill Book Company, 1962).

6. E. Gatti and V. Svelto, Nuclear Instruments and Methods 4 (1959) 189.

7. B. E. Bonner, M. A. Thesis Physics Rice University (1963) 9.

8. W. E. Mott and R. B. Sutton, Handbook of Physics, Sec. 14, 145-147.

9. H. W. Fullbright and J. Verba, Proc. Rutherford Jubilee Int. Cong. (Manchester, 1961).

10. Robley D. Evans, The Atomic Nucleus (McGraw-Hill Book Company, 1955) 317.

11. B. V. Rybakov and V. A. Sidorov, Fast Neutron Spectroscopy, (Consultants Bureau Inc., New York).

V. ACKNOWLEDGEMENTS

The author wishes to thank Dr. G. C. Phillips for initiating the time-of-flight experiments which led to the construction of the time-of-flight system described in this thesis and for his guidance throughout the course of the experiments.

Appreciation is expressed to James Buchanan for aid in developing the equipment and to B. E. Bonner, D. L. Bernard, Dr. C. Poppelbaum, Dr. A. S. Divatia and the other members of the fast neutron group at the Bonner Nuclear Laboratory of Rice University for the many long hours spent in the accumulation of data.

Appreciation is also expressed to the United States Atomic Energy Commission and Rice University for the support of the research program.